

NAL Proposal No. 615
Correspondent: J. E. Pilcher
Enrico Fermi Institute
University of Chicago
Chicago, IL 60637
Telephone: 312-753-8747

A Study of the Forward Production of
Massive Particles

C. Adolphsen, K. J. Anderson, K. Karhi, J. E. Pilcher, E.I. Rosenberg
Enrico Fermi Institute, University of Chicago

and

K. T. McDonald, A. J. S. Smith
Princeton University

November 8, 1978

A Study of the Forward Production of Massive Particles

1. Introduction

An important class of hadron reactions remains largely unexplored by modern high sensitivity, high resolution experiments. These are reactions which proceed through non-diffractive t-channel exchanges to produce a high-mass particle in the forward direction. Although the cross sections are in the nanobarn range these processes have unique kinematic features which may substantially improve the signal-to-background levels compared with the much-studied region near $x = 0$. The kinematics is also well suited to high sensitivity studies where a selective trigger is essential.

The proposed experiment is designed to use a beam of 10^{10} pions/pulse and offers ~ 8 % acceptance for two body decays within the accepted mass bite. This yields a sensitivity of about 2400 events/picobarn in a 1000 hr. run. The mass resolution is 0.5%.

We propose to use a high flux pion beam at 50 GeV and to study the mass spectrum from 1 to 4 GeV/c². The 2-body final states $K\pi$, $p\bar{p}$, lepton-hadron, and lepton-lepton would be detected.

Although the experiment is a sensitive search in a relatively unexplored kinematic region, there are some obvious reactions of interest. These include $\pi N \rightarrow DC$ (associated production of a charmed meson and charmed baryon) and $\pi N \rightarrow \eta_C N$. The rate of detected events is estimated to be over 100 events/hour both reactions. The former reaction is of particular interest since if it were detected with sufficient cross section the charmed baryon mass spectrum could be studied by missing mass techniques.

2. Apparatus

The detector exploits the fact that the forward going particle carries almost all the energy of the incident beam and is produced with a transverse momentum of only a few hundred MeV/c. Thus the P_T of the decay products is largely determined by the mass of the parent.

The detector consists of two parts, shown schematically in Fig. 1. The first part magnetically selects pairs of particles in a mass region of interest while the second part analyzes the pair-mass with high resolution and identifies the mass of each track.

The mass selecting system is shown in detail in Fig. 2. It is a set of dipoles located just after the target which causes secondaries of a given P_T to cross the beam axis a fixed distance downstream. Since the secondaries from the 2-body decays of interest have nearly equal and opposite P_T both particles cross the beam axis at the same downstream point (~ 9 m from the target). An adjustable collimating slit ~ 20 cm x 60 cm aperture is located at this point. The mass of the selected system is determined by the fields in the magnets while the accuracy is determined by the slit aperture in the bend plane. The transverse position of a particle at the slit is given by

$$x = \frac{L}{P_L} (P_T - \frac{\Delta P_T}{2})$$

where ΔP_T and L are the P_T -kick and length of the dipole system and P_T and P_L are the transverse and longitudinal momenta of the particle.

The downstream face of the mass selecting system is well shielded except for the small exit aperture. A hevimet plug is located in the neutral secondary beam, half-way through the dipoles, to protect the analyzing spectrometer from neutrals. The plug is far enough downstream so it does not intercept the non-interacting beam. This beam is bent to one side and transported downstream to a dump behind the detector. An important feature

of this system is that no detector element of the downstream spectrometer views the target directly.

The mass selection system has been designed with standard ANL beam-line dipoles. The gap height in the four magnets is 6-in., 15-in., 22.5-in., and 30-in. to accommodate the divergence in the non-bend plane.

Downstream from the mass slit is a high resolution spectrometer. The exact design will depend on the magnet available. Figure 1 shows a design based on a magnet with a 2-m wide aperture, a 1-m high gap and a P_T -kick of 0.5 GeV/c. For a given mass setting of the upstream magnets two regions 60 cm by 1 m are illuminated on the entrance aperture of the analyzing magnet. The position of these regions varies with the mass setting.

It should be noted that for the trigger, the momentum of tracks entering the analyzing spectrometer is already closely correlated with position.

Thus fairly precise requirements on the mass and total momentum of the triggering pair can be imposed at the trigger level. It would be expected to have a two level trigger, the first using standard NIM electronics and the second based on a custom digital processor. The data acquisition system would be designed to handle ~1000 events/pulse.

Gas Cerenkov counters are used for π , K, \bar{p} separation. A lepton identifier is placed at the downstream end of the detector.

The mass resolution of the system is limited by multiple scattering in the 0.2 absorption length beryllium target to ~ 7 MeV/c at the D mass.

3. Beam

A high flux pion beam with good spot size is required. The new M1 beam is particularly attractive. It appears that at a momentum as low as 50 GeV/c the horizontal and vertical acceptance of this beam can be each doubled by using a tune with half the wavelength of the standard tune. This increases the low momentum flux by at least a factor of 4 and leads to a

yield at 50 GeV/c of over 10^{10} /pulse for 5×10^{12} interacting protons. If fluxes larger than this are available the momentum bite of the beam would be reduced.

Muons are a potentially serious problem with this beam and must be carefully handled. At 50 GeV/c over 20% of the pions and 80% of the kaons decay in the first 960 feet. Spoilers are probably required and possibly a sharp bend just before the target.

4. Rates

The acceptance of the mass selection system is determined for the reaction $\pi N \rightarrow DC$ by Monte Carlo calculation, using the t-distribution $\downarrow \rightarrow K\pi$ estimated by Field and Quigg of $e^{-3.5 t}$. We find an 8% acceptance.

Assuming that the analyzing spectrometer has complete acceptance for these events the event rate/hour/picobarn of production cross section ($B\sigma$) is:

$$\frac{10^{-36} (\text{cm}^2/\text{pb}) \times (2 \times 10^9) (\text{interacting } \pi/\text{pulse}) \times 300 (\text{pulse/hr}) \times 0.08 (\text{acceptance})}{20 \times 10^{-27} (\text{cm}^2)}$$

= 2.4 ev/pb/hr.

Thus in a 1000 hour experiment one could hope to collect 2400 events per picobarn.

The total cross section for $\pi N \rightarrow DC$ where C is any system with a mass less than $3.5 \text{ GeV}/c^2$ is estimated by Field and Quigg to be 2.5 nb at $E_{\text{inc}} = 50 \text{ GeV}$. This yields an event rate from D's in the $K\pi$ channel of

$$2500 \text{ pb} \times 0.018 (\text{probability of D to } K\pi) \times 2.4 \text{ ev/hr/pb}$$

= 108 events/hr.

It should be noted however that the cross section to particular charmed baryon channels are estimated to be ~ 300 times smaller.

The $K\pi$ coincidence background is a major concern and is very difficult to estimate. The contribution from one exclusive channel, namely $\pi p \rightarrow K^*(1780)n$ $\downarrow K\pi$ is estimated to be 400 pb if 1% of this cross section lies in the mass bite of interest⁽²⁾. The contribution through this channel from the K-component of the beam is about 15% of the above due to the small fraction of kaons which reach the target.

We are investigating methods to improve the signal to background ratio for D production in the $K\pi$ channel. One possibility is the Fitch method of detecting a coincident pion arising from $D^* \rightarrow D^0\pi$. The Q-value in this decay is only about 6 MeV so that the pion comes off close to the D^* direction. In this experiment the pion would be detected by bringing it out in a channel through the spacer plates used to open up the gaps of the mass selecting dipoles.

A second interesting reaction with cross section estimates available⁽¹⁾ is $\pi p \rightarrow \eta_c n$. If one assumes that $|\langle \frac{u\bar{u} + d\bar{d}}{\sqrt{2}} | \eta_c \rangle|^2$ is 1% as suggested, then $\sigma(\pi p \rightarrow \eta_c n) \sim 80$ nb at 50 GeV. If the branching ratio of η_c to $p\bar{p}$ is taken to be the same as the J/ψ (2×10^{-3}) then the event rate is

$$80 \times 10^3 \text{ (pb)} \times (2 \times 10^{-3}) \times 2.4 \text{ (ev/pb)} \\ = 380 \text{ events/hr.}$$

5. Request

We request 1000 hours of data taking in a 50 GeV pion beam with 10^{10} pions/pulse and a good spot size. The latter is necessary for good mass resolution. We would need the mass selecting and analyzing magnets, an on-line computer system and PREP electronics. We would expect to supply the PWC's, scintillator hodoscopes, Cerenkov counters, and special triggering logic.

6. Conclusion

This experiment would explore a unique class of reactions which have received little attention at Fermilab. It is designed to exploit the high sensitivities offered by the high flux pion beams. The experiment is sensitive to several reactions of current topical interest as well as having more general capabilities. In particular the mass spectrum of lepton-hadron final states is largely unstudied and could reflect semi-leptonic decays of a more massive system.

REFERENCES

1. R. D. Field and C. Quigg, Estimates of Associated Charm Production Cross Sections, Fermilab -75/15- THY.
2. S. U. Chung et al., Phys. Rev. Letters 40, 355 (1978).

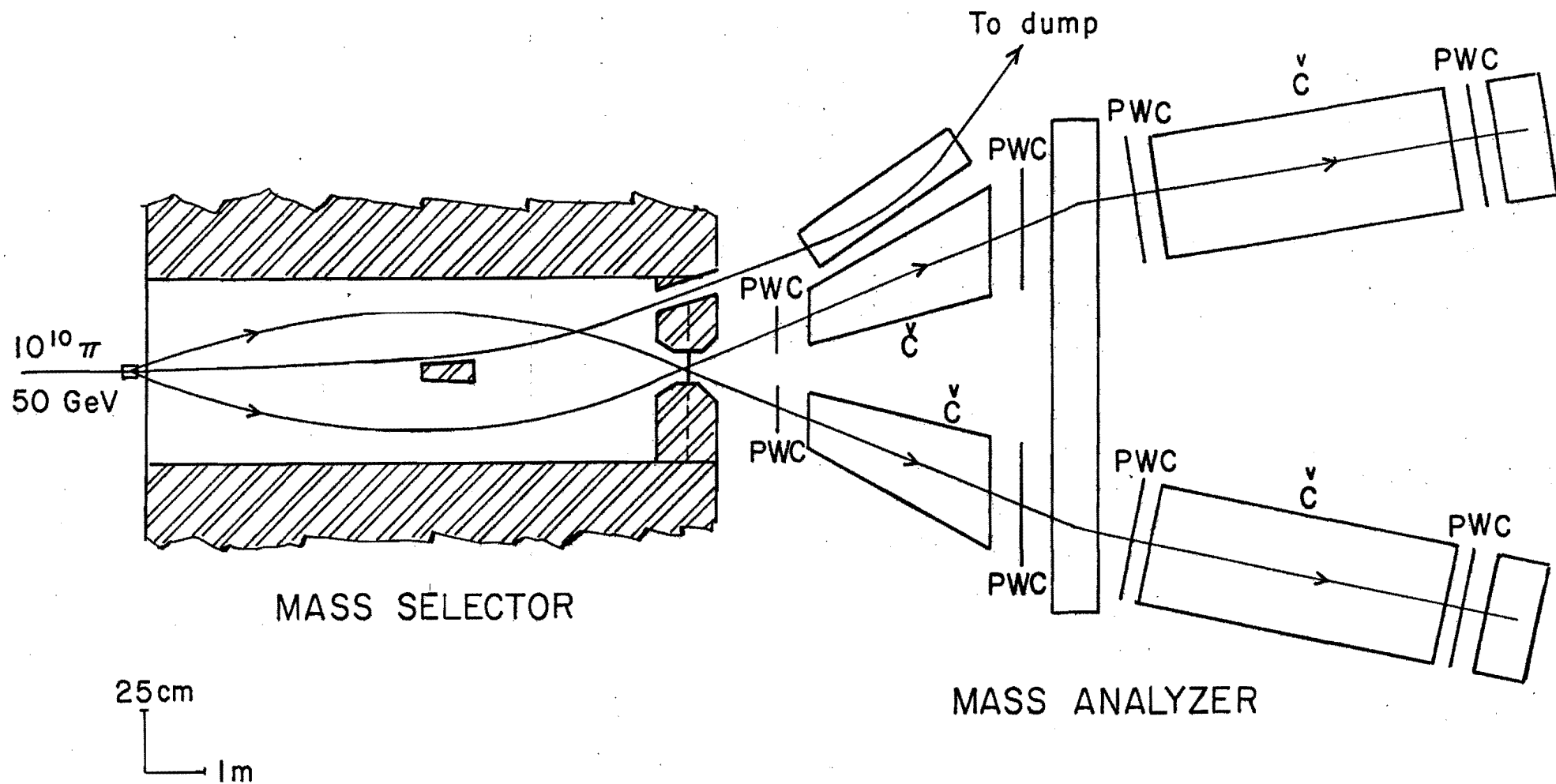
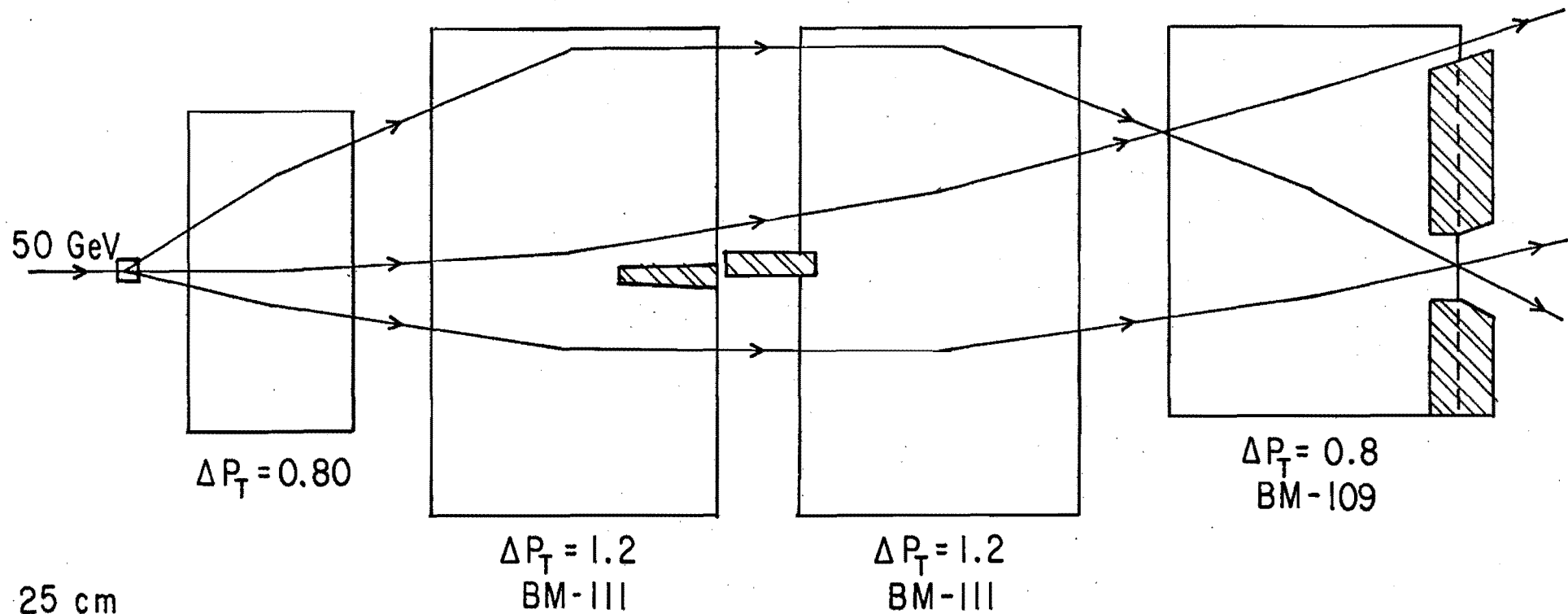


Figure 1



TRAJECTORIES FOR MASS $4 \text{ GeV}/c^2$
 $X_1 = 0.25$, $X_2 = 0.67$

Figure 2

ADDENDUM TO PROPOSAL 615

A First Phase to Study Forward Produced μ -pairs

C. Adolphsen, J. Alexander, K.J. Anderson, K. Karhi,

J. E. Pilcher, E. I. Rosenberg

Enrico Fermi Institute, University of Chicago

and

J. Elias

Fermi National Accelerator Laboratory, Batavia, Illinois 60510

and

K. T. McDonald, A.J.S. Smith

Joseph Henry Laboratories, Princeton University, Princeton, NJ 08540

May 4, 1979

ADDENDUM TO P-615

I. INTRODUCTION

There have been a number of developments in P-615 since its review by the PAC.

First, we find that the P-West beam would be acceptable and the overall cost of the experiment would be reduced by a factor of ~ 2.5 from earlier estimates of the Meson Department. The details are outlined below.

Second, new physics results have come to light which suggest that an important first phase of the experiment is a study of μ -pairs produced in the forward direction. This measurement is technically easier than the hadron pair study and the physics issues are well defined. A desire to study this channel was expressed in the original proposal although the case was not developed. We are still very much interested in forward hadron pairs but would propose this as a Phase II study. Presently approved experiments are poorly suited to study forward μ -pairs because they contain toroidal field geometries and/or beam dumps which lead to poor acceptance at large x_F .

II. PHYSICS MOTIVATION

There is mounting evidence that μ -pair production in πN interactions occurs through quark-antiquark annihilation. If this is the mechanism, it offers a method of measuring the quark structure function of the pion. Tests of the model and a structure function determination were done in Fermilab's E-444.^{1,2} The structure function is obtained from a measurement of the cross section in terms of Feynman- x of the μ -pair (x_F) and the pair mass M . The x -values of the two annihilating quarks (x_1 and x_2) are given by energy-momentum conservation, neglecting transverse momenta, as

$$x_1 x_2 = M^2/s$$

$$x_1 - x_2 = x_F$$

Berger and Brodsky³ have pointed out that in the kinematic region where the x of the quark from the pion (x_1) becomes large, the quark goes off shell.

More explicitly, the quark's Q^2 goes like $k_T^2/(1-x_1)$ where k_T is the quark transverse momentum. Thus the kinematic region $x_1 \rightarrow 1$ probes the "far-off-shell, short distance internal dynamics of the hadron wave function."³ It is reasonable to expect that in this high momentum transfer limit one may understand the process in terms of a model based on QCD.

Berger and Brodsky invoke a simple model involving single-gluon exchange between the valence quarks of the pion. They conclude that the cross section for the $\pi N \rightarrow \mu^+ \mu^- + \dots$ should go like

$$(1-x_1)^2 (1+\cos^2\theta) + \frac{4}{9} \langle k_T^2 \rangle / M^2 \sin^2\theta$$

in the large x_1 region. The first term is the scaling component of the cross section and corresponds to transverse polarization of the virtual photons. The second term is explicitly scale breaking and is identified with longitudinal polarization.

These predictions have been compared with the E-444 data. If a $\sin^2\theta$ component develops in the angular distribution for large x_1 and if the distribution is fit by $1 + \alpha \cos^2\theta$, α should decrease as x_1 becomes large. Figure 1 shows the angular distribution for three different lower bounds on x_F . Since the data fall very rapidly with x_F the mean value of x_F for each plot is close to the lower bound. Moreover, since M^2 and s are fixed, x_1 increases with x_F . The anticipated trend is observed. In Fig. 2 the value of α is plotted as a function of x_F and compared with the predictions of the model for two different masses. The data themselves are characterized by a mass of ~ 4 GeV. The data are consistent with expectations.

In our recent publication² we find a good phenomenological fit to the structure function at large x by the form $(1-x)^1$. We have tried the alternative form suggested by Berger and Brodsky of

$$\bar{q}(x) \sim (1-x)^2 + \frac{2}{9} \langle k_T^2 \rangle \frac{1}{M^2}$$

and obtain an equally good representation. The value obtained for $\langle k_T^2 \rangle$ is ~ 1.2 GeV in agreement with expectations.

We conclude that existing data is in accord with the model.

Obviously better quality data at high x is indicated, especially since this is the region where quantitative understanding may be possible. If we are ever to test QCD it must be in a relatively clean situation, such as this, where one mechanism is expected to dominate. Theoretical work is underway at SLAC to determine the extent to which the model predictions reflect the basic assumptions of QCD and how other effects might enter.

To observe clearly the scale breaking term requires good acceptance at large x_F . In addition it is important to have good acceptance in $\cos\theta$ to isolate the structure function components associated with transverse and longitudinal photon polarization. The general form of the cross section in terms of structure functions, even in the forward direction, is much more complicated than the predictions of this simple model.⁴

To evaluate existing detectors for such a study we note that at $M=8$ GeV, $E_{inc} = 250$ GeV the two terms in the structure function given above are equal at $x_1 = 0.94$, or $x_F = 0.8$. For an exactly symmetric μ -pair with ($\cos\theta = 0$) and with zero p_T the muons have a lab angle of 32 mr. For $\cos\theta = 0.5$ the angle is 16 mr. The lower limit of the acceptance in E-326 is 30 mr and in Telegdi's CERN experiment, it is 32 mr. The acceptance in E-605 is limited to $x_F \lesssim 0.5$ because of the beam dump.⁵ These acceptance difficulties are reduced at higher masses but as we will see below the small production cross section at high x_F precludes the use of much higher masses.

III. APPARATUS

We propose to use the apparatus described in P-615 with a hadron filter installed in the mass selector magnets. Figure 3 shows the detector. A nuclear target of ~50% interaction probability would be used just upstream of the mass selector. At a later stage a hydrogen/deuterium target might be used but this is not envisaged at the present time. A drift distance of ~1 m. separates the target from the filter to permit isolation of the production point during analysis.

(1) Hadron Filter

The filter would be a low Z material such as beryllium or carbon of as short a length as is consistent with an acceptable downstream counting rate. Detailed studies of this length are now underway but if the filter were beryllium extending 8.5 meters (23 absorption lengths), then the charged hadron flux at the downstream face with the magnetic field off would be $\sim 2 \times 10^6$ for 10^{10} incident pions at 100 GeV.⁶ A high density carbon filter gives the same flux but leads to a 35% deterioration in mass resolution. We expect that the field will further reduce the charged hadron flux and that distance between the shield and detectors will effectively reduce the rates.

(2) Muons in the Beam

To avoid the muon component of the beam we divide the detector elements at beam height and provide a gap in the median plane. The height of the gap grows with distance from the target to match the divergence of the beam (~ 1 mr). The multiple scattering angle of beam muons at 75 GeV (the lowest energy we expect to use), induced by the hadron filter is 1.0 mr.

(3) Mass Selection Magnets

A collimator at the downstream end of the mass selector, as described in P-615, is suitable for studying hadron pairs but is of no value when muons are involved. It would be removed. In this mode of operation the mass selector sweeps out low p_T and low x_F muons and hence provides a cutoff on low mass pairs. Higher mass pairs are accepted with an efficiency of $\sim 20\%$ at $M = 8$ GeV and $x_F = 0.9$ for a 250 GeV beam. The higher mass acceptance is limited by the width of the mass selector magnets. The efficiency falls to $\sim 10\%$ at $M = 11$ GeV.

(4) Muon Background from Hadron Decay and Low Mass Pairs

We have done a Monte Carlo calculation to estimate the muon flux through the detector from the decay of hadrons produced in the target and hadron filter. Production cross sections for π^\pm, K^\pm were parameterized as a function of x_F and p_T . Muons from the decays of these hadrons were tracked through the mass selection magnets, including the flux return yokes. With the selector magnets energized at 18 Kg and 2×10^9 interacting pions of 250 GeV we find that the detector sees 6×10^4 single muons from hadron decay.

To estimate the muon flux from low mass μ -pair production we have used our own measurements from E-331. With the same conditions as above we find that the detector sees 4×10^3 single muons from pairs and 240 low mass pairs. The tracks of the pairs diverge sharply and can be easily identified and eliminated using the trigger logic of the downstream spectrometer.

We conclude that muon fluxes from these sources are entirely acceptable. Without the sweeping of the mass selection magnets these fluxes would be more than two orders of magnitude larger.

(5) Muon Halo of the Beam

Our colleagues with the E-326 experiment have made detailed studies of the muon halo in P-West. They conclude that with a beam energy of 200 GeV and 10^{13} incident protons, the muon halo is $\sim 10^6/m^2$. This flux is manageable but accidental triggers involving halo muons must be guarded against.

(6) Acceptance and Resolution

As outlined below an important aspect of the experiment involves measuring the pion structure function with data of two different mass values but the same M^2/s . This involves masses of 4 GeV at 75 GeV incident energy and masses of 7.3 GeV at 250 GeV incident.

Shown in Figures 4 and 5 are the acceptances at two different

incident energies as a function of x_F , p_T , and the CM decay angles $\cos\theta$ and ϕ . In the large x_F region of interest, the efficiency is 20% at the higher energy and 8% at the lower setting. These are very substantial values for the interaction rate employed.

The mass resolution is dominated by multiple scattering in the hadron filter. We estimate a mass resolution with a carbon filter of ~ 150 MeV and roughly independent of pair mass. This resolution depends on fitting the pair trajectories to a common production point as was done in E-331 and E-444.

IV. MEASUREMENT STRATEGY

The goal of the study is to measure the pion structure function with high precision at large x . The method is set out in our recent publications from E-444.² It amounts to measuring

$$\frac{d^2\sigma}{dx_1 dx_2} = \frac{4\pi\alpha^2 s}{9M^4} f^\pi(x_1) g^N(x_2) \quad , \quad x_1 x_2 = M^2/s$$

$$x_1 - x_2 = x_F$$

where $f^\pi(x_1) = x\bar{u}^\pi(x_1)$

and $g^N(x_2) = \frac{4}{9} x_2 u^N(x_2) + \frac{1}{9} x_2 \bar{d}^N(x_2)$

It is of particular interest here to isolate the scale breaking term in $f^\pi(x_1)$ predicted by QCD ($1/M^2$ term). This is done by measuring the pion structure function using data with at least two different masses. Unless care is taken the nucleon structure function contributes differently at different masses since $x_1 x_2 = M^2/s$. To avoid uncertainties associated with the nucleon structure, one must keep x_2 fixed by varying s with M^2 . Thus the scale breaking term is isolated by subtracting structure functions measured at different M and s but fixed M^2/s . We would propose to take data at $E_{inc} \sim 75$ GeV and $E_{inc} \sim 250$ GeV and to determine the structure function from data with $M \sim 4$ at 75 GeV and $M \sim 4 \times \sqrt{250/75} = 7.3$ GeV at 250 GeV. If the scale breaking term varies like $1/M^2$, its size changes by a factor of 3.3. Figure 6 shows the expected errors on the structure function measured at the two different beam energies if Berger and Brodsky's analysis is correct. The statistical errors correspond to 600 hours at $E_{inc} = 250$ GeV and 200 hours at $E_{inc} = 75$ GeV with 10^{13} incident protons per pulse, and 300 pulses per hour.

V. COSTS

The cost of the experiment is substantially reduced by using the P-West beam and experimental area. Costs directly attributable to the MI location which would not apply in P-West amount to \$830K, leaving \$484K according to the Meson Department's impact statement. John Peoples indicates that the

spectrometer analyzing magnet may be considered as Research Division equipment and not charged explicitly to this experiment. This reduces the cost to \$324K. Most of this is in the mass focusing magnets and we are working with Ron Fast toward further reductions. Inevitably there will be some added costs unique to P-West. Thornton Murphy is investigating the adequacy of presently installed power. Should more power be needed, he estimates ~\$180K for installation and bus work.

The physics disadvantages of P-West appear tolerable. The hadron pair mass resolution would be degraded by 30% because of the larger beam spot. Since the beam has a smaller total bend, muon halo is more troublesome although it appears that careful work with spoilers as done for E-326 can make it acceptable.

Additional costs not contained in present estimates include an on-line computer, PREP electronics and the hadron filter.

The requested amount of running time is 1000 hours.

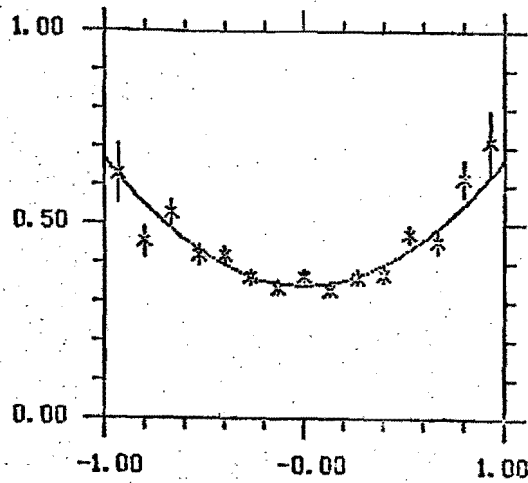
VI. CONCLUSIONS

The study of pion induced μ -pairs in the forward direction is an important first phase for the detector. This kinematic region is one of the most interesting, yet existing detectors have poor capability here. In the proposed study, this experiment will be able to exploit the full potential of the P-West pion beam with good resolution and good acceptance.

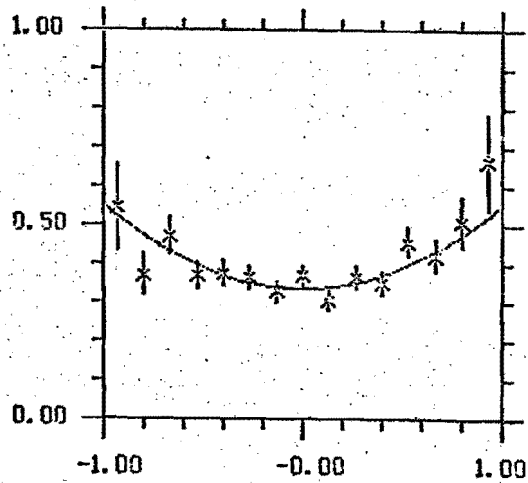
REFERENCES

1. Comparison of Muon-Pair Production to the Quark-Antiquark Annihilation Model, G. E. Hogan et al., Phys. Rev. Lett. 42, 948 (1979) [copy attached]
2. Determination of the Pion Structure Function from Muon-Pair Production, C. B. Newman et al., Phys. Rev. Lett. 42, 951 (1979) [copy attached]
3. Quark Structure Functions of Mesons and the Drell-Yan Process, E. L. Berger and S. J. Brodsky, Phys. Rev. Lett. 42, 940 (1979) [copy attached]
4. C. S. Lam and Wu-Ki Tung, Phys. Rev. D 18, 2447 (1978).
5. L. M. Lederman, private communication.
6. High Energy Particle Interactions in Large Targets, A. Van Ginneken and M. Awschalom, Fermilab Report.

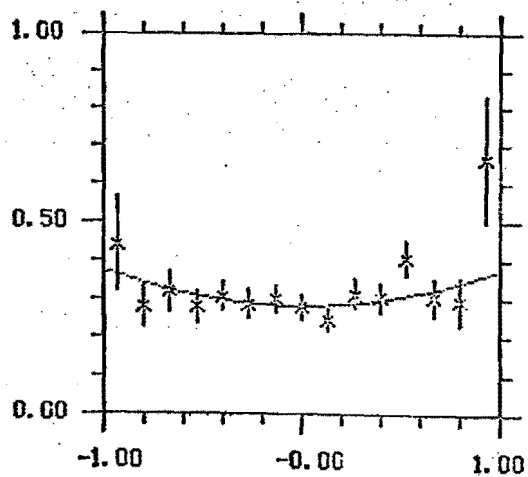
$\pi^- N \rightarrow M^+ M^- X$ AT 225 GeV/c
 $M_{M^+ M^-} > 3.5$ GeV $(1 + \alpha \cos^2 \theta)$ FITS



$x_F > 0.0$
 $\alpha = 0.95 \pm 0.11$



$x_F > 0.5$
 $\alpha = 0.65 \pm 0.16$



$x_F > 0.63$
 $\alpha = 0.34 \pm 0.21$

Figure 1. Results from E-444 on decay angular distributions versus x_F .

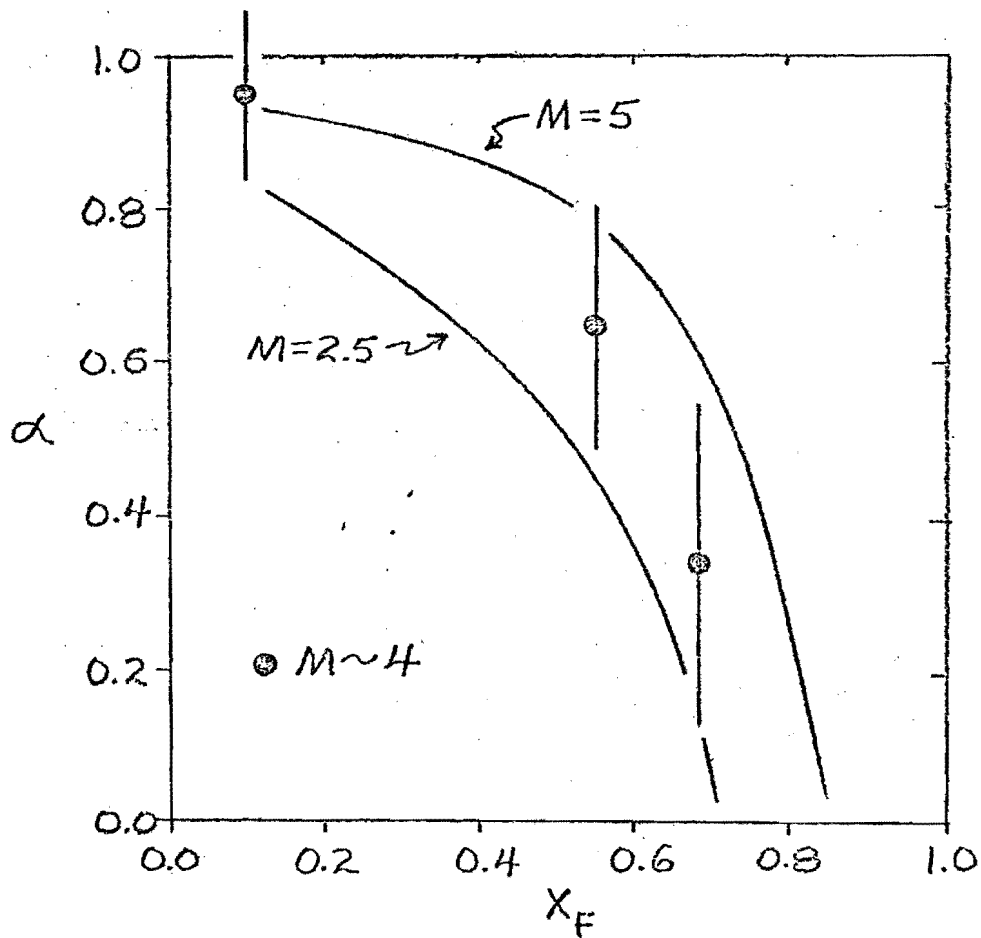


Figure 2. Angular distribution parameter α as a function of x_F compared with the model predictions of Berger and Brodsky. The data are characterized by a mean mass of 4 GeV.

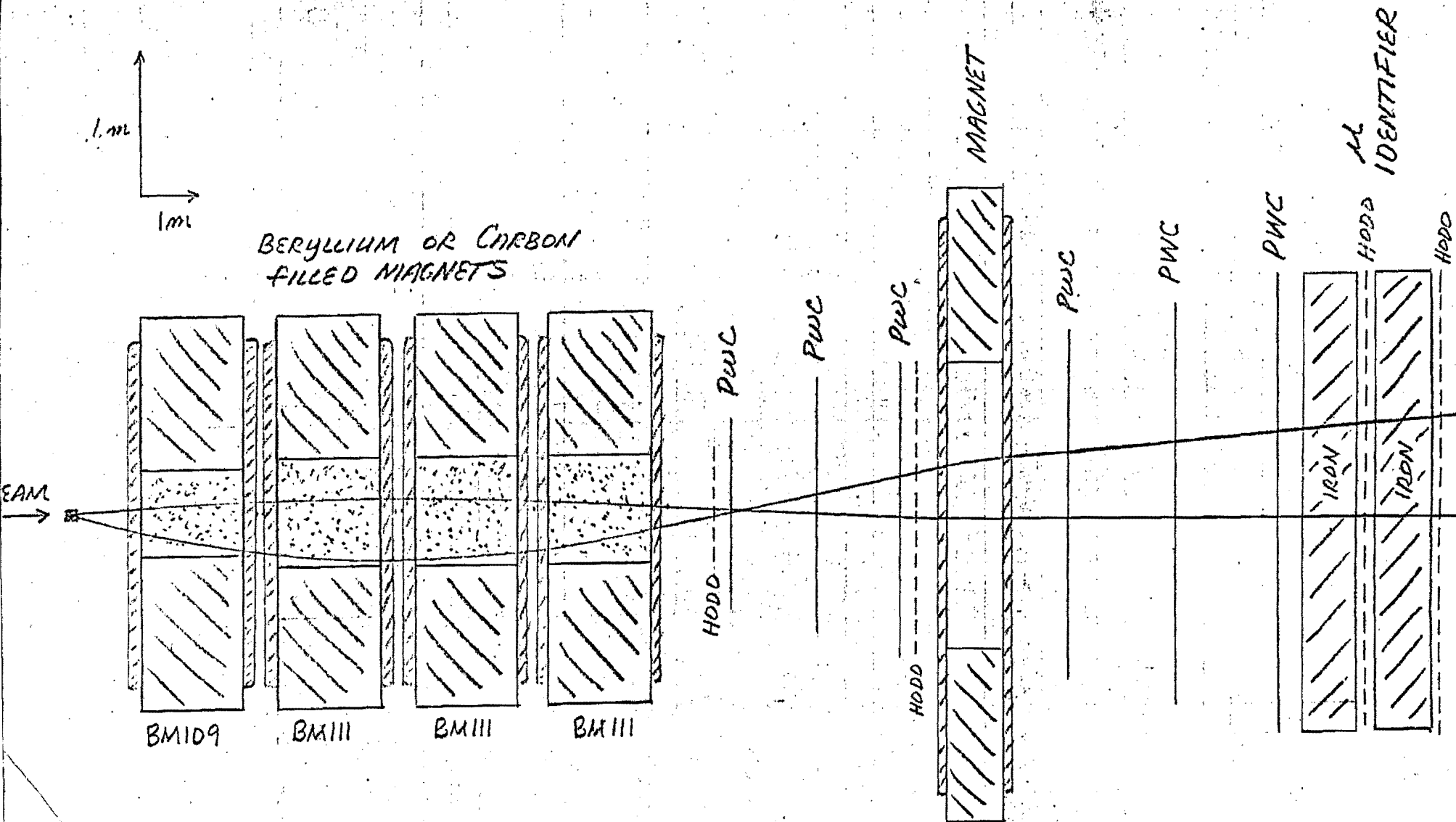


Figure 3.

Figure 4. Detection efficiency at a mass of 8 GeV and an incident energy of 250 GeV.

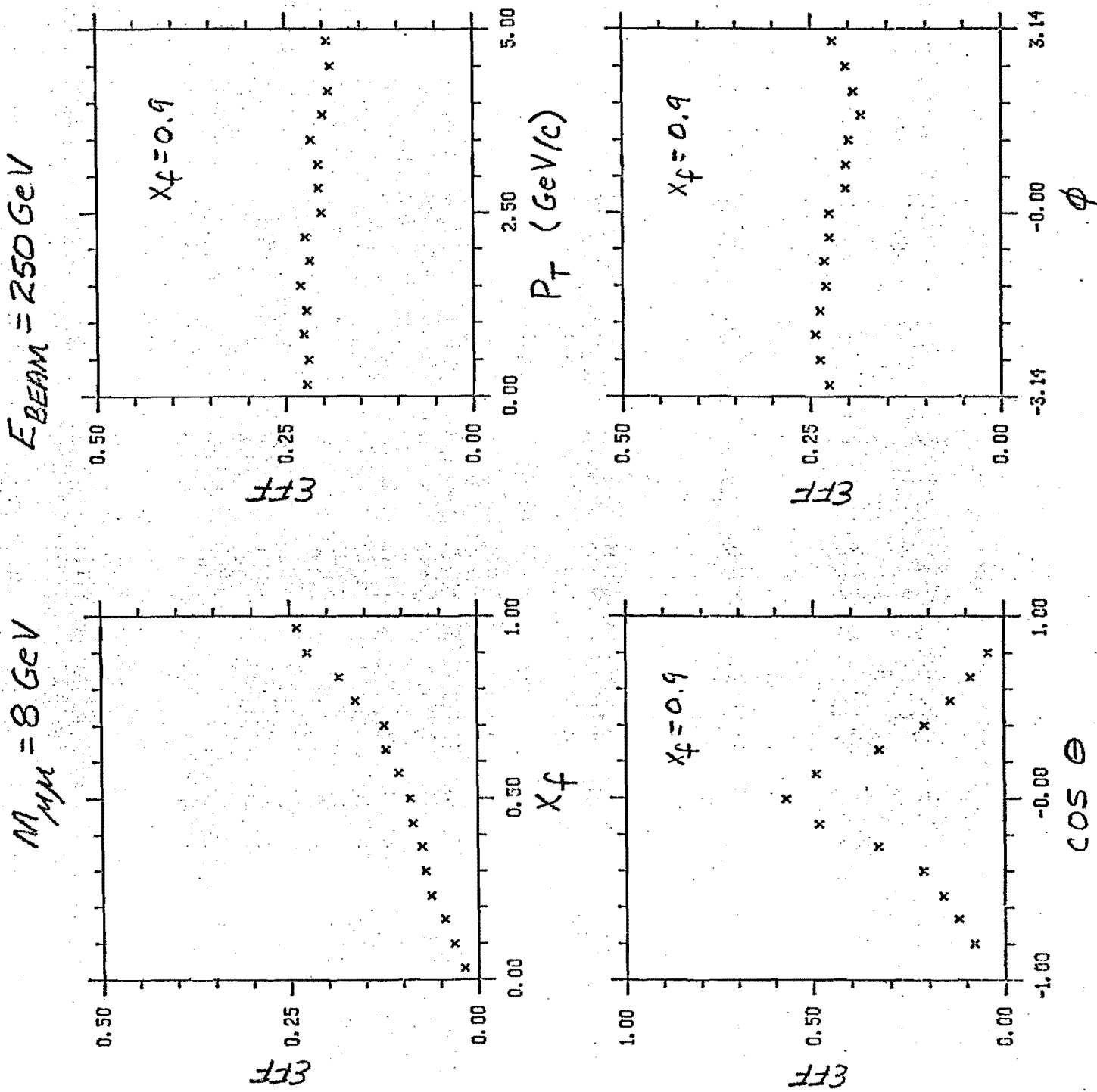
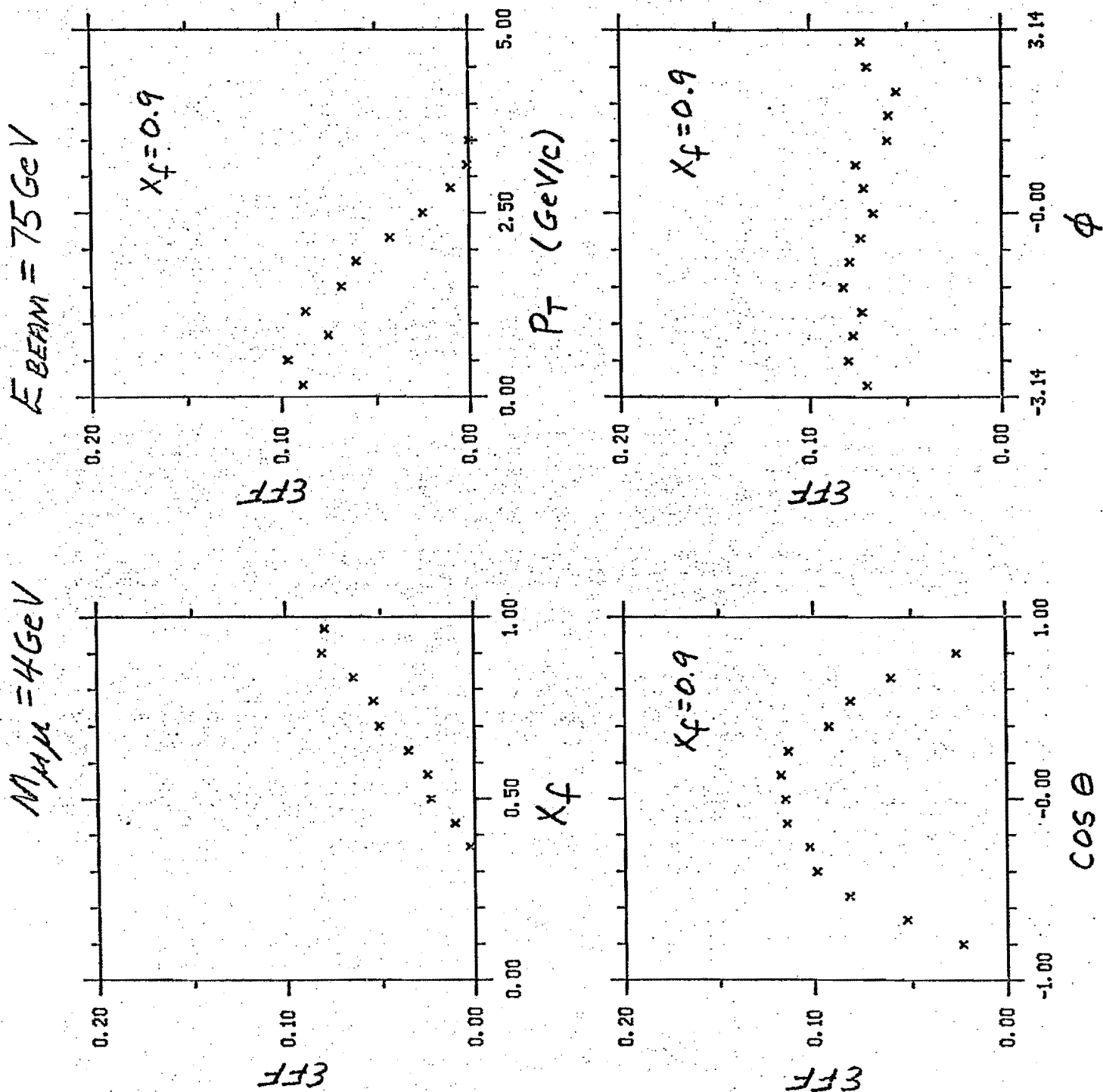


Figure 5. Detection efficiency at a mass of 4 GeV and an incident energy of 75 GeV.



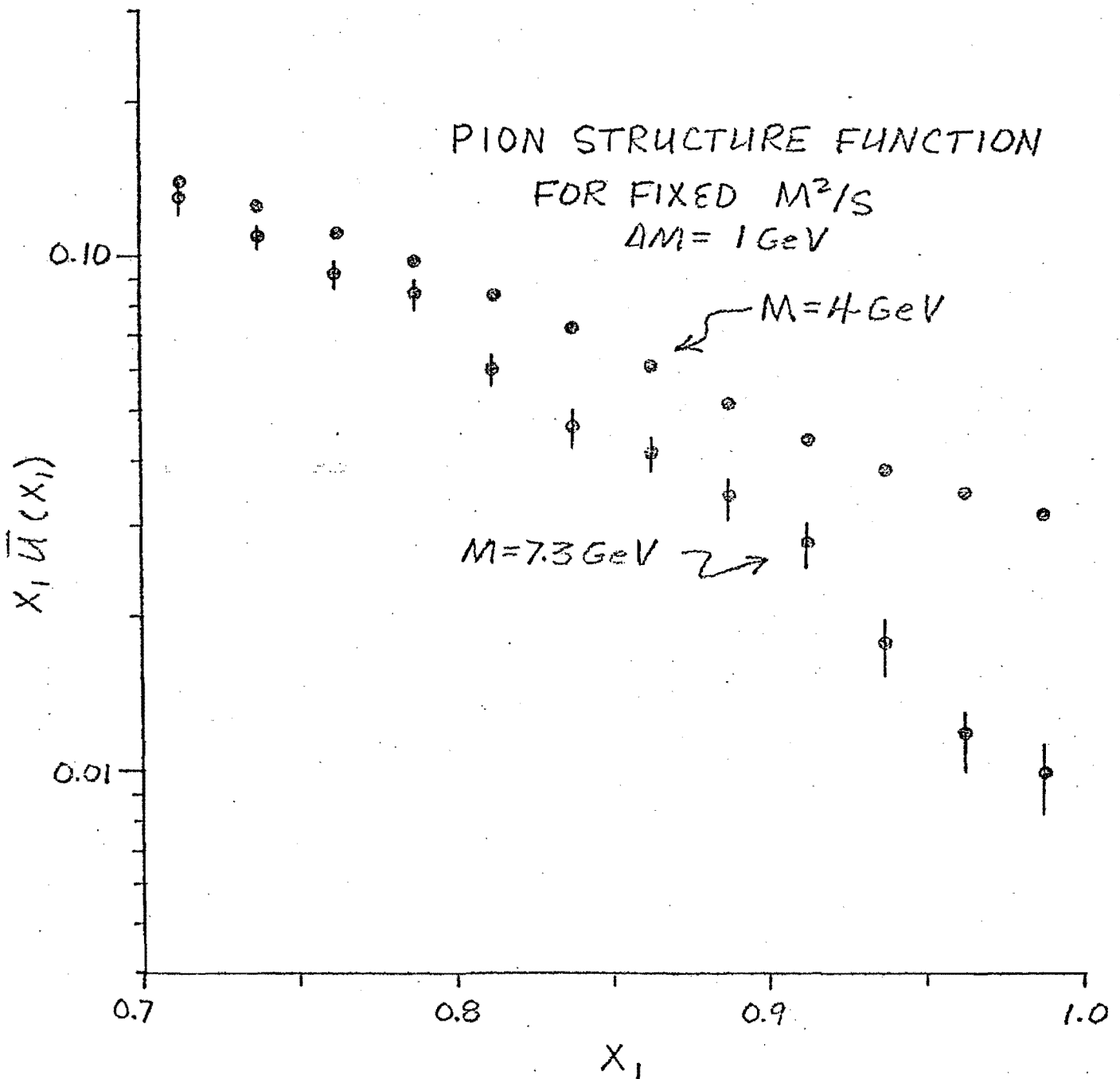


Figure 6. Expected precision on the pion structure function. The dependence on mass is scale breaking. The curves shown are for the model of Berger and Brodsky.

Comparison of Muon-Pair Production to the Quark-Antiquark Annihilation Model

G. E. Hogan, K. J. Anderson, R. N. Coleman,^(a) K. P. Karhi, K. T. McDonald,
C. B. Newman, J. E. Pilcher, E. L. Rosenberg, G. H. Sanders,^(b)
A. J. S. Smith, and J. J. Thaler

Enrico Fermi Institute, University of Chicago, Chicago, Illinois 60637, and University of Illinois, Urbana, Illinois 61801, and Joseph Henry Laboratories, Princeton University, Princeton, New Jersey 08540

(Received 22 January 1979)

New data on muon-pair production at 225 GeV/c by π^- , π^+ , and proton beams are analyzed with regard to the production mechanism. The observed spin alignment of the pair and the dependence of the cross section on beam-particle type are strong indications that the production is through electromagnetic quark-antiquark annihilation.

The preceding Letter¹ discussed the general features of production of high-mass μ pairs by 225-GeV/c beams of π^- , π^+ , and protons on C, Cu, and W targets. In this article we discuss aspects of the data in the context of a theoretical framework.

The general formalism of lepton-pair produc-

tion by hadrons via a virtual intermediate photon has been discussed in the literature.² An important special case is the description in terms of quark-antiquark annihilation, first proposed by Drell and Yan and further developed by other authors.³ The μ -pair production cross section for interacting hadrons A and B, neglecting p_T and including three colors is

$$\frac{d\sigma^2}{dM dx_F} = \frac{8\pi\alpha^2}{9M^3} \sum_i \frac{e_i^2}{x_1+x_2} [x_1 f_i^A(x_1) x_2 f_i^B(x_2) + x_1 f_i^A(x_1) x_2 f_i^B(x_2)], \tag{1}$$

where $x_{1,2} = [\pm x_F + (x_F^2 + 4M^2/s)^{1/2}]/2$ are the momentum fractions (Feynman x) of the annihilating quarks in the projectile and target hadrons, $x f_i^A(x)$ is the momentum spectrum for quarks (antiquarks) of flavor i (\bar{i}) in hadron A. $x_F \equiv 2P_L^*/\sqrt{s}$ in this analysis, where P_L^* is the μ -pair longitudinal momentum in the overall center of mass. Thus, the observed mass and Feynman- x (x_F) spectra for the data reflect the distributions of the annihilating quarks.

This mechanism predicts striking differences for the lepton-pair production cross section in nucleon-nucleon scattering compared to pion-nucleon scattering. In the nucleon-nucleon case the interacting particles contain no valence antiquarks and only antiquarks from the $q\bar{q}$ sea can contribute. Since the probability density functions for the sea quarks fall steeply with x_1 and x_2 the observed mass spectrum should fall rapidly with mass for fixed x_F . Incident pions, on the other hand, contain a valence antiquark which has a significant probability of being found at large x_1 . Thus, the cross section for pion-induced pairs should fall more slowly with mass than for incident protons.

To permit comparison of π^- - and proton-induced cross sections at the highest possible mass values, we have used the proton results of Yoh *et al.*⁴ The cross-section ratio is shown in Fig. 1. The π^- to proton cross-section ratio

rises to over 100 at a mass of 10 GeV/c² in dramatic agreement with expectations.

Consider next the comparison of the π^- - and π^- -induced μ -pair production cross sections. In this case, valence quarks and antiquarks from

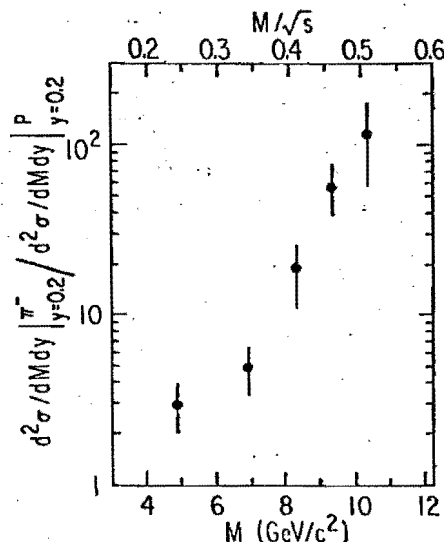


FIG. 1. The ratio of π^- -induced to proton-induced μ -pair cross section at $y_{c.m.} = 0.2$ as a function of mass. Proton data at 225 GeV/c has been calculated from the scaling observed in 200-, 300-, and 400-GeV/c data of Ref. 4.

the interacting particles should dominate production if x_1 and x_2 are both large. In this experiment, a carbon target was used so that the target is exactly symmetric in u - and d -quark distributions ($u^p = d^n, d^p = u^n$). In the case of an incident π^- the valence antiquark is a \bar{u} with charge $-\frac{2}{3}$ while for an incident π^+ it is a \bar{d} with charge $\frac{1}{3}$. Since the pair production varies as the square of the quark charge, one expects $\sigma(\pi^+C \rightarrow \mu^+\mu^- \dots) / \sigma(\pi^-C \rightarrow \mu^+\mu^- \dots)$ to be $\frac{1}{4}$. If x_1 and x_2 are not both large, sea antiquarks can contribute and the cross-section ratio approaches 1 as x_1 and x_2 approach 0. Figure 2(a) shows the measured π^+/π^- cross-section ratio as a function of pair mass for $x_F > 0$. It is seen to be near unity for the J/ψ as might be expected for strong production from charge-symmetric initial states. As the pair mass increases above $3.1 \text{ GeV}/c^2$ the ratio is consistent with a fall toward $\frac{1}{4}$. Any deviation of the ratio from unity is indicative of an electromagnetic process and the limiting value of $\frac{1}{4}$ is predicted by the $q\bar{q}$ annihilation mechanism.

The solid line in Fig. 2(a) is a calculation of the π^+/π^- cross-section ratio from the pion and nucleon structure functions together with the contribution of the observed resonances. The determination of the pion structure function is discussed in the following Letter.⁵ Since π^+ and π^- structure functions are the same, the approach

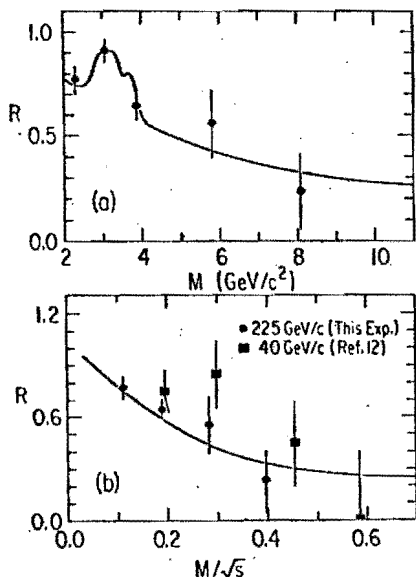


FIG. 2. (a) $R = \sigma(\pi^+C \rightarrow \mu^+\mu^-X) / \sigma(\pi^-C \rightarrow \mu^+\mu^-X)$ vs $M_{\mu\mu}$ at $225 \text{ GeV}/c$. The solid curve is described in the text. (b) R vs M/\sqrt{s} for data at 225 and $40 \text{ GeV}/c$ (Cu target) for continuum pairs. The curve is the same as shown in (a) but with resonance production excluded.

to $\frac{1}{4}$ is primarily dependent on the nucleon structure functions and in particular on the form of the nucleon sea-quark distributions. Using the measured sea-quark distributions of Kaplan *et al.*,⁶ we find reasonable agreement with the data although these sea-quark distributions have been determined only for $x_2 > 0.25$.

Figure 2(b) shows the π^+/π^- ratio from this experiment as a function of M/\sqrt{s} , together with other measurements.

Two variables, in addition to M , x_F , and p_T are required to specify the μ -pair final state. Natural choices are the polar (θ^*) and azimuthal angles of one of the muons in the μ -pair rest frame. The annihilation of two massless spin- $\frac{1}{2}$ on-shell fermions to a 1^- intermediate state would lead to a $1 + \cos^2\theta^*$ distribution, where θ^* is measured from the $q\bar{q}$ direction in the μ -pair c.m. system. If the p_T of the final-state μ -pair is zero, the beam and target define the $q\bar{q}$ direction. If p_T is nonzero, the $q\bar{q}$ direction is not determined. Collins and Soper⁷ have suggested using the vector which bisects the angle between the beam and the reverse of the target vector as the best average estimate of the $q\bar{q}$ direction.

The distribution of the polar (helicity) angle has been examined for mass regions below the J/ψ ($2.0 < M < 2.7 \text{ GeV}/c^2$), the J/ψ ($2.7 < M < 3.5 \text{ GeV}/c^2$), and above the J/ψ ($M > 3.5 \text{ GeV}/c$). The distributions are shown in Fig. 3 with their best fits to the form $1 + \lambda \cos^2\theta^*$. Results of the fits are given in Table I. The continuum region above

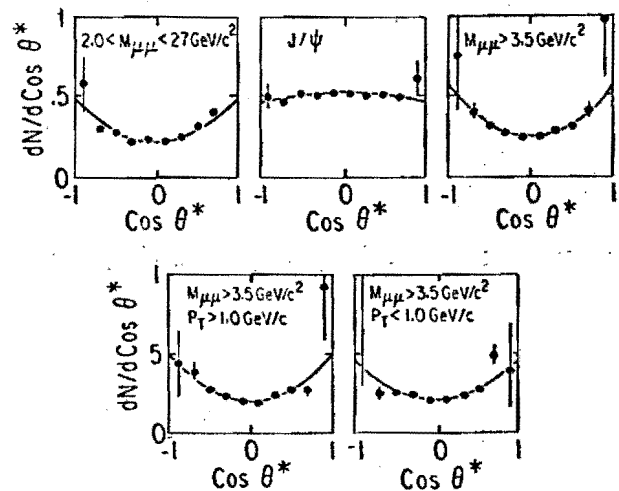


FIG. 3. Helicity angular distributions in three different mass intervals. The $M > 3.5 \text{ GeV}/c^2$ interval is also shown divided in two p_T intervals. The Collins-Soper angle (θ^*) is defined in the text.

TABLE I. Helicity angular distribution fits (DF means degrees of freedom).

Data interval		Fit results			
Mass (GeV/c ²)	p_T (GeV/c)	Flat χ^2/DF	$1 + \cos^2\theta^*$ χ^2/DF	$1 + \lambda \cos^2\theta^*$ λ	χ^2/DF
2.0-2.6	All	79.7/9	25.6/9	1.14 ± 0.17	25.0/8
J/ψ	All	7.0/9	212.0/9	-0.10 ± 0.05	4.7/8
>3.5	All	44.6/9	6.6/9	1.30 ± 0.23	4.7/8
>3.5	<1.0	31.6/9	12.6/9	1.17 ± 0.29	12.2/8
>3.5	>1.0	36.4/9	11.2/9	1.47 ± 0.39	8.8/8

and below the J/ψ shows strong evidence of the expected spin alignment. The J/ψ data are consistent with a flat angular distribution. The mass dependence of these distributions reflects a clear change in the underlying production mechanism for the J/ψ compared with the continuum. Similar results for the continuum are also obtained using either the s -, t -, or u -channel reference directions for the helicity angle.

A number of attempts have been made to explain the broad p_T spectra for the μ pair in terms of quantum-chromodynamic corrections to the Drell-Yan mechanism.⁸ The corrections are expected to be most significant at higher p_T and may modify the helicity angular distribution. Figure 3 and Table I give the helicity angular distribution for transverse momenta above and below 1 GeV/c. Evidence for spin alignment and a value of λ consistent with 1.0 are seen in both p_T intervals.

Equation (1) implies the scaling result that $M^3 d\sigma/dM$ is a function only of M^2/s . It should be noted that this is not an especially unique feature of the annihilation mechanism since such a result also follows from dimensional arguments and has been found to apply also to the production of some narrow resonances.⁹ Nevertheless, it is a condition which should be satisfied by the data.

Figure 4(a) shows our $\pi^- N \rightarrow \mu^+ \mu^- X$ data compared with measurements at lower energies. This scaling prediction is not well satisfied by currently available π^- data. However, some caution should be exercised in interpreting this result. The mass region covered by the low-energy experiments is below the J/ψ where nonscaling resonance or continuum production may contribute. In this lower-mass region both $\langle p_T \rangle$ and the A dependence are observed to vary with mass,¹ while they do not for the mass region of this experiment. A clear lack of scaling or an experi-

mental discrepancy is observed in the comparison with data of Ref. 13.

As a consistency check Fig. 4(b) shows our proton-induced cross sections in comparison

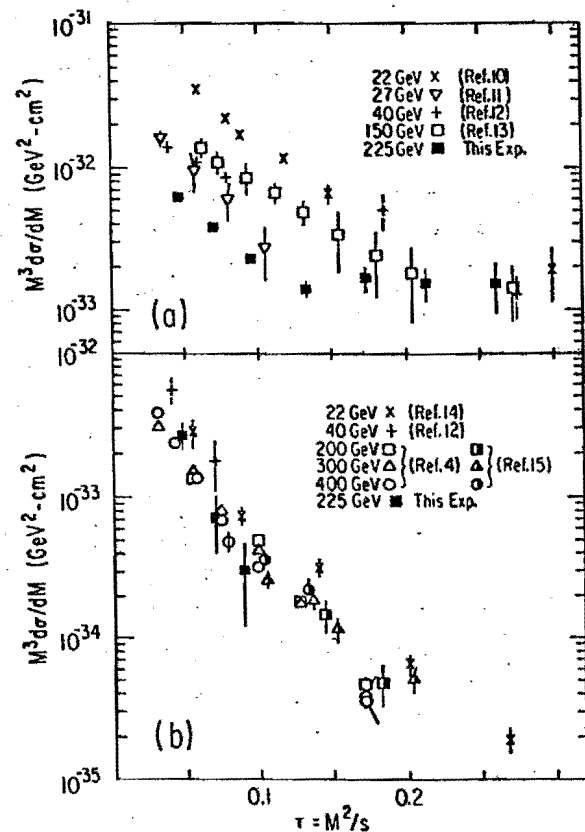


FIG. 4. $M^3 d\sigma/dM$ vs M^2/s , the scaling form of the cross section for (a) $\pi^- N \rightarrow \mu^+ \mu^- X$ and (b) $p N \rightarrow \mu^+ \mu^- X$. Data from Refs. 4 and 15 are converted from the measured $[d^3\sigma/dM dy]_{y=0}$ to $d\sigma/dM$ ($x > 0$) by using the antiquark functions reported by the authors of Ref. 6 together with valence-quark distributions from deep-inelastic lepton scattering. The resulting x_F distributions agree well with the observed spectrum in this experiment.

with other measurements. They are in good agreement and scaling is reasonably well satisfied.

The annihilation model also predicts scaling in the ratio of the π^+ - to π^- -induced μ -pair production cross sections. The data are shown in Fig. 2(b). The ratio is consistent with being a function of M^2/s only.

In conclusion, we have performed a number of new tests of the Drell-Yan annihilation mechanism. The observed spin alignment of the μ pair and the strong dependence of the cross section on beam-particle species are in striking agreement with the hypothesis that the production proceeds through an electromagnetic quark-antiquark annihilation.

This work was performed at the Fermi National Accelerator Laboratory and supported by the U. S. Department of Energy and National Science Foundation.

^(a)Present address: University of Rochester, Rochester, N. Y. 14627.

^(b)Present address: Los Alamos Scientific Laboratory, Los Alamos, N. M. 87545.

¹K. J. Anderson *et al.*, preceding Letter [Phys. Rev. Lett. **42**, 944 (1979)].

²R. C. Oakes, *Nuovo Cimento* **44A**, 440 (1966); C. S. Lam and Wu-Ki Tung, *Phys. Rev. D* **18**, 2447 (1978).

³S. D. Drell and T.-M. Yan, *Phys. Rev. Lett.* **25**, 316, 902(E) (1970), and *Ann. Phys.* **66**, 578 (1971). For a recent discussion see the review of T.-M. Yan, in Pro-

ceedings of the Eighth International Symposium on Multiparticle Dynamics, Kaysersberg, France, 1977, edited by R. Arnold, J. B. Gerber, and P. Schubella (Centre National de la Recherche Scientifique, Strasbourg, France, 1977).

⁴J. K. Yoh *et al.*, *Phys. Rev. Lett.* **41**, 684 (1978).

⁵C. B. Newman *et al.*, following Letter [Phys. Rev. Lett. **42**, 951 (1979)].

⁶D. M. Kaplan *et al.*, *Phys. Rev. Lett.* **40**, 435 (1978); L. M. Lederman, in Proceedings of the Nineteenth International Conference on High Energy Physics, Tokyo, Japan, 1978 (to be published). Use of the alternative [non-SU(3) symmetric] fit of the nucleon sea-quark distribution functions does not significantly affect the results.

⁷J. C. Collins and D. E. Soper, *Phys. Rev. D* **16**, 2219 (1977).

⁸See, for example, E. L. Berger, in *New Results in High Energy Physics—1978*, AIP Conference Proceedings No. 45, edited by R. S. Panvini and S. E. Csorna (American Institute of Physics, New York, 1978); F. Halzen and D. M. Scott, University of Wisconsin Report No. COO-881-21, 1978 (to be published).

⁹T. K. Gaisser *et al.*, *Phys. Rev. D* **15**, 2572 (1977).

¹⁰J. Alspector *et al.*, in Proceedings of the Nineteenth International Conference on High Energy Physics, Tokyo, Japan, 1978 (to be published), Reports No. BNL-OG 419 and No. UR-659/COO-202.

¹¹S. B. Golovkin *et al.*, in Proceedings of the Nineteenth International Conference on High Energy Physics, Tokyo, Japan, 1978 (to be published).

¹²M. J. Corden *et al.*, *Phys. Lett.* **76B**, 226 (1978).

¹³M. A. Abolins *et al.*, in Proceedings of the Nineteenth International Conference on High Energy Physics, Tokyo, Japan, 1978 (to be published).

¹⁴L. M. Lederman and B. G. Pope, *Phys. Lett.* **66B**, 486 (1977).

¹⁵D. Antreasyan *et al.*, *Phys. Rev. Lett.* **39**, 906 (1977).

Determination of the Pion Structure Function from Muon-Pair Production

C. B. Newman, K. J. Anderson, R. N. Coleman,^(a) G. E. Hogan, K. P. Karhi, K. T. McDonald, J. E. Pilcher, E. I. Rosenberg, G. H. Sanders,^(b) A. J. S. Smith, and J. J. Thaler
Enrico Fermi Institute, University of Chicago, Chicago, Illinois 60637, and University of Illinois, Urbana, Illinois 61801, and Joseph Henry Laboratories, Princeton University, Princeton, New Jersey 08540

(Received 22 January 1979)

Data on muon-pair production by pions are used to determine the momentum distribution for valence quarks in the pion. The shape of a nucleon structure function is also obtained and is compared with a calculation based on existing data.

In the two preceding Letters,¹ we have presented features of high-mass muon-pair production and compared the data with predictions from a quark-antiquark annihilation model. In this Letter, the data are used within the framework of the model to obtain the momentum spectrum of valence quarks in the charged pion.

The general form of the Drell-Yan cross section² in terms of the quark distribution functions is given in Ref. 1. There are a number of simplifications in its application to this experiment. For a pion it follows from charge conjugation and isospin invariance that the quark distribution function is the same for both valence quarks. Fur-

ther, if the kinematic region is restricted to $M > 4 \text{ GeV}/c^2$ ($x_1 > 0.25$), the contribution of sea quarks in the pion is expected to be negligible.³ Then for pion-nucleon collisions the sum over quark flavors reduces to two terms corresponding to the two valence quarks in the pion. The Drell-Yan cross section for π^-N interactions and colored quarks becomes

$$\frac{d^2\sigma}{dM dx_F} = \frac{8\pi\alpha^2}{9M^3(x_1+x_2)} x_1 \bar{u}^{\pi}(x_1) \times \left[\frac{4}{9} x_2 u^N(x_2) + \frac{1}{9} x_2 \bar{d}^N(x_2) \right] \quad (1)$$

or

$$M^2 \frac{d^2\sigma}{dx_1 dx_2} = \frac{4\pi\alpha^2 s}{9} f^{\pi}(x_1) g^N(x_2), \quad (2)$$

where $f^{\pi}(x_1) \equiv x_1 \bar{u}^{\pi}(x_1)$ and $g^N(x_2) \equiv \frac{4}{9} x_2 u^N(x_2) + \frac{1}{9} x_2 \bar{d}^N(x_2)$.

Since $M^2/s = x_1 x_2$, the cross section as a function of x_1 and x_2 is predicted to factor into a function of x_1 times a function of x_2 . Equation (2) is used to test the factorization hypothesis and to deduce the functions $f^{\pi}(x_1)$ and $g^N(x_2)$. To use Eq. (2), data with $4 < M < 8.75 \text{ GeV}/c^2$ and $x_F > -0.05$ are binned in a rectangular grid of x_1 and x_2 . Higher-mass pairs are excluded to avoid possible contributions from unresolved resonances (T, T'). Figure 1 shows the distribution of events in the x_1 - x_2 plane. The range of x_1 ($0.25 < x_1 < 1.0$) is divided into fourteen bins and the range of x_2 ($0.05 < x_2 < 0.28$) divided into nine bins. The 85 populated bins are fitted with the form of Eq. (2), yielding fourteen values of $f^{\pi}(x_1)$ and

nine values of $g^N(x_2)$. We find a χ^2 of 65 for 61 degrees of freedom indicating good agreement with the factorization hypothesis.

Only the normalization of the product $f^{\pi}(x_1) \times g^N(x_2)$ is measured in this type of experiment. Additional information is required to fix the normalization of the pion structure function. The target-nucleon function $g^N(x_2)$, cannot be normalized directly to data from deep-inelastic lepton-scattering experiments because such experiments measure a different linear combination of quark distribution functions. Several authors⁴ have extracted the individual nucleon quark distribution functions using fits to deep-inelastic lepton-scattering data with the q^2 dependence expected from quantum chromodynamics. In addition, a nucleon sea-quark distribution has been determined by Kaplan *et al.*⁵ Over the interval $0.05 < x_2 < 0.28$, we normalize $g^N(x_2)$ to $\frac{4}{9} x_2 u^N(x) + \frac{1}{9} x_2 \bar{d}^N(x)$, where the u -valence-quark distribution is taken from Buras and Gaemers⁴ with $q^2 = -m^2$, and the u and \bar{d} sea-quark distributions are taken from Ref. 5. In Fig. 2, the normalized nucleon structure function is shown together with the expected form. The agreement in shape is excellent.⁶ For comparison, Fig. 2 also shows the expected function if both valence- and sea-quark distributions are taken from Ref. 4. If these curves were used to normalize $g^N(x_2)$ the normalization would be 20% smaller. A comparison of the resulting data points with these shapes would have a χ^2 confidence level of 6%.

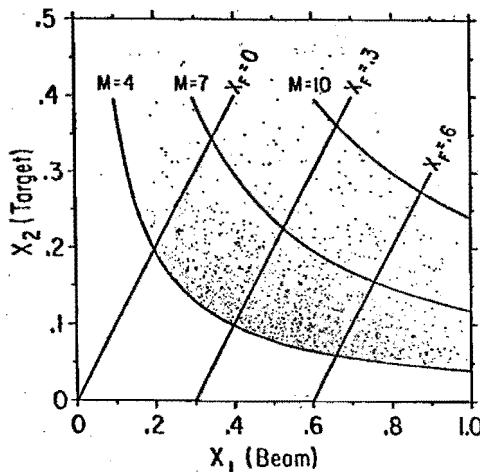


FIG. 1. Distribution of events in the x_1 - x_2 plane. Lines of constant x_F ($x_F = x_1 - x_2$) and M ($x_1 x_2 = M^2/s$) are also shown.

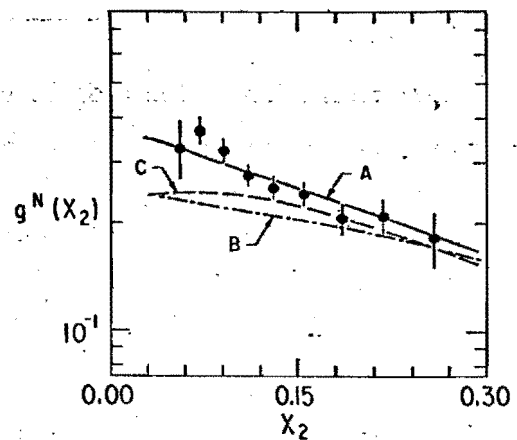


FIG. 2. The nucleon structure function $g^N(x_2) = \frac{4}{9} x_2 u^N(x_2) + \frac{1}{9} x_2 \bar{d}^N(x_2)$ averaged over protons and neutrons in the C, Cu, and W targets. Curve A is used to normalize the data points and is described in the text. Curve B is from Buras and Gaemers, Ref. 4. Curve C is from Fox, Ref. 4.

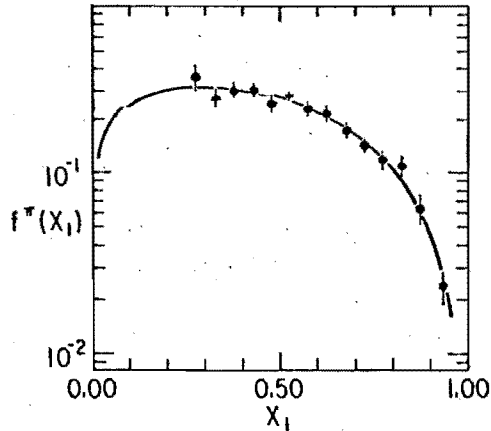


FIG. 3. The pion structure function $f^{\pi}(x_1) = x_1 \bar{u}^{\pi}(x_1)$.

The pion structure function is shown in Fig. 3. It has been fitted with the forms⁷ $x_1 \bar{u}^{\pi}(x_1) = ax_1^{1/2} \times (1-x_1)^b$ and $x_1 \bar{u}^{\pi}(x_1) = a(1-x_1)^b$. The parameters for these and other fits discussed below are summarized in Tables I and II. Theoretical predictions for the exponent b are in the range 0–2.0.⁸ It should be noted that the errors shown in Figs. 2, 3, and Tables I and II reflect only statistical uncertainties. An overall normalization uncertainty of 20% should also be applied to allow for A -dependence uncertainties and other systematic effects.

Using the values for a and b from fit 1 in Table I, we obtain, including normalization uncertainties,

$$\int_{0.25}^{1.0} x \bar{u}^{\pi}(x) dx = 0.14 \pm 0.03,$$

$$\int_{0.25}^{1.0} \bar{u}^{\pi}(x) dx = 0.31 \pm 0.07.$$

If the fit is used to extrapolate these results to $x_1 = 0$, the integrals are 0.20 ± 0.05 and 1.11 ± 0.27 , respectively, for $0 < x_1 < 1.0$. The first integral represents the fraction of the pion momentum carried by the \bar{u} valence quark in the pion. Since both pion valence quarks have the same distribu-

TABLE II. Nucleon-structure-function fits: χ^2 per degree of freedom (χ^2/DF) for fit to normalization curve of Fig. 2.

	χ^2/DF
$4.0 < M < 8.75$, all p_T	5.1/8
$4.0 < M < 6.0$, all p_T	6.6/8
$5.0 < M < 8.75$, all p_T	0.5/6
$4.0 < M < 8.75$, $p_T < 1.0$	10.4/8
$4.0 < M < 8.75$, $p_T > 1.0$	7.5/8

tion function, the first integral indicates that about 40% of the pion momentum is carried by valence quarks.

The second integral provides a sum-rule check and a test of the color hypothesis. This integral over $0 < x_1 < 1$ is expected to be 1 since a π^- contains one \bar{u} valence quark. If quarks were colorless it would be 3 since $\bar{u}(x)$ was obtained through the use of Eq. (1). The value obtained is consistent with 1, but is sensitive to the unobserved low- x behavior of $\bar{u}^{\pi}(x)$.

As a consistency check, the pion and the nucleon structure functions obtained above can be used to calculate the μ -pair cross section as a function of mass and x_F using Eq. (2). Figure 4 shows the results of such a calculation compared to the data. The curves, calculated from the structure functions of Figs. 2 and 3, are in good agreement with the data. The inset to Fig. 4(a) shows the structure function applied to the whole mass range $M < 9 \text{ GeV}/c^2$. It falls below the data by a factor of 2 at $2 \text{ GeV}/c^2$ and a factor of 15 at $0.6 \text{ GeV}/c^2$.

We have investigated the sensitivity of our results to transverse-momentum and mass dependence by performing the structure function fit in different kinematic regions. The results are summarized in Table I. The variation of the pion structure function is described by the parameters from the fit to the form $ax_1^{1/2}(1-x_1)^b$. To gauge

TABLE I. Pion-structure-function fits.

	Fit	a	b
$4.0 < M < 8.75$, all p_T	$a\sqrt{x_1}(1-x_1)^b$	0.90 ± 0.06	1.27 ± 0.06
$4.0 < M < 6.0$, all p_T	$a\sqrt{x_1}(1-x_1)^b$	0.93 ± 0.07	1.30 ± 0.07
$5.0 < M < 8.75$, all p_T	$a\sqrt{x_1}(1-x_1)^b$	0.81 ± 0.10	1.23 ± 0.11
$4.0 < M < 8.75$, $p_T < 1.0$	$a\sqrt{x_1}(1-x_1)^b$		1.17 ± 0.08
$4.0 < M < 8.75$, $p_T > 1.0$	$a\sqrt{x_1}(1-x_1)^b$		1.21 ± 0.09
$4.0 < M < 8.75$, all p_T	$a(1-x_1)^b$	0.52 ± 0.03	1.01 ± 0.05

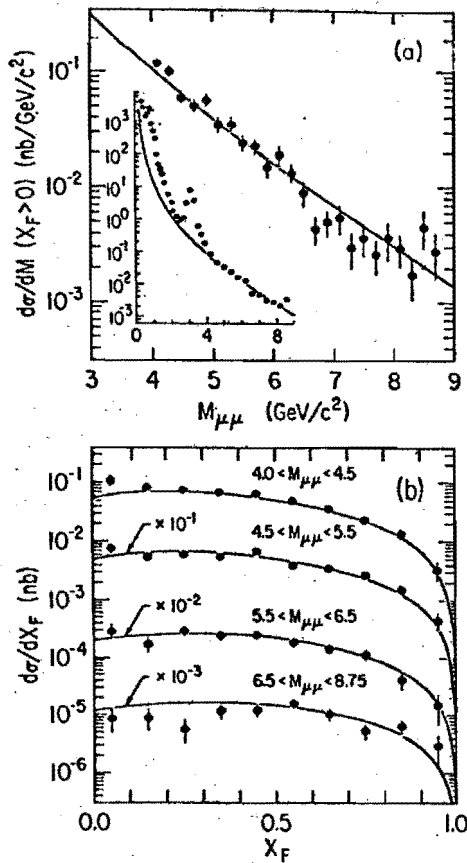


FIG. 4. Data from Ref. 1 are compared with expectations based on the structure functions determined from these same data (solid line). (a) Mass spectrum $d\sigma/dM$ vs M . The inset shows the extrapolation of the structure function to lower-energy measurements (Ref. 1 of Ref. 1), with the additional constraint that $x_F > 0.1$. (b) Feynman- x distribution $d\sigma/dx_F$ vs x_F .

the sensitivity of the nucleon function to mass and p_T effects, we give the χ^2 for the fit of the nucleon structure function to the calculated function shown in Fig. 2 (see Table II).

In mass, the intervals $4.0 < M < 6.0$ GeV/c² and $5.0 < M < 8.75$ GeV/c² were used. The mean mass in the lower interval is 4.7 GeV/c² while that in the upper interval is 6.0 GeV/c². No significant variation in either the pion or nucleon structure function was observed with mass. The fit was performed in two p_T regions: $p_T < 1.0$ and $p_T > 1.0$ GeV/c. The pion function is the same in both cases, within statistics. The nucleon function is slightly flatter in the higher- p_T region.

The effect of Fermi motion has been investigated with a Monte Carlo calculation.⁹ It changes the power of the pion function by 0.02 and has a negligible effect on its normalization. It should

be noted that the structure-function results depend on the applicability of Eq. (2), and as noted in the preceding Letter,¹ existing data are not in good agreement with the scaling prediction of the model.

In conclusion, we have used data on the pion production of μ pairs and the colored quark-anti-quark annihilation model to determine the pion quark distribution function for the region $x > 0.25$. The shape of the nucleon structure function obtained is in good agreement with expectations. To 10% accuracy the pion quark distribution function shows no evidence for dependence on mass or p_T in the kinematic range of this experiment. The fraction of the pion momentum carried by its two valence quarks is comparable to the fraction of nucleon momentum carried by three valence quarks.

We are pleased to acknowledge the cooperation of the Fermilab Neutrino Department. Special thanks are due Jack Steinberger and the CERN-Heidelberg collaboration who loaned us the large multiwire proportional chamber detectors used in the upstream part of the spectrometer.

This work was performed at the Fermi National Accelerator Laboratory and supported by the U. S. Department of Energy and the National Science Foundation.

^(a) Present address: University of Rochester, Rochester, N. Y. 14627.

^(b) Present address: Los Alamos Scientific Laboratory, Los Alamos, N. M. 87545.

¹K. J. Anderson, this issue [Phys. Rev. Lett. 42, 944 (1979)]; G. E. Hogan *et al.*, preceding Letter [Phys. Rev. Lett. 42, 948 (1979)].

²S. D. Drell and T.-M. Yan, Phys. Rev. Lett. 25, 316, 902(E) (1970).

³We have estimated the effect of the pion sea by assuming it has the form $f_{\pi^+}(x) = 0.1(1-x)^5$ as suggested by G. R. Farrar [Nucl. Phys. B77, 429 (1974)] and R. D. Field and R. P. Feynman [Phys. Rev. D 15, 2590 (1977)]. If the pion sea is included parametrized in this way, the normalization of the pion valence-quark distribution function decreases by about 4%.

⁴A. J. Buras and K. J. F. Gaemers, Nucl. Phys. B132, 249 (1978); G. Fox, Nucl. Phys. B131, 107 (1977), together with private communication.

⁵D. M. Kaplan *et al.*, Phys. Rev. Lett. 40, 435 (1978).

⁶Figure 2 differs from previously reported results, K. J. Anderson *et al.*, University of Illinois Report No. EFI 78-38R (to be published), for the target-nucleon structure function. The fitting procedure has been improved since the earlier report.

⁷If the fit is to be extrapolated outside the region of

measurement, the square-root form is preferable since it leads to a finite value for the integral of the valence-quark function $u(x)$ over the range $0 \leq x \leq 1$. Several authors have suggested that the pion structure function should approach zero as \sqrt{x} . See, for example, P. V. Landshoff and J. C. Polkinghorne, Nucl. Phys. B19, 432 (1970); J. Kuti and V. F. Weisskopf, Phys. Rev. D 4, 3418 (1971).

⁸S. D. Drell and T.-M. Yan, Phys. Rev. Lett. 24, 181 (1970); G. B. West, Phys. Rev. Lett. 24, 1206 (1970); Farrar, Ref. 3; G. Altarelli *et al.*, Nucl. Phys. B92, 413 (1975); A. Donnachie and P. V. Landshoff, Nucl. Phys. B112, 223 (1976); Field and Feynman, Ref. 3.

⁹We use the momentum distribution for particles in the nucleus of R. D. Amado and R. M. Woloshyn, Phys. Rev. Lett. 36, 1435 (1976).

energy [Eq. (7)]. We do not discount contributions from kinks and phonons but merely assert their small weight for \hat{S}_{cc} in contrast to the other spectral densities, as considered in Ref. 1.

To summarize, the present and our previous study¹ have revealed that all three fundamental normal modes of the sine-Gordon equation, the linear phonon mode, the nonlinear kink, antikink, and breather modes give rise to resonances in the thermalized sine-Gordon chain. In particular, although the breather is a well-documented solution to the continuous and deterministic problem,^{2,3,5,6} it has not previously been shown that these coherent anharmonic phonon effects persist in statistical mechanics or they have the strong response characteristic shown here. In view of the lack of any method providing reliable estimates of the spectral densities of such nonlinear systems, we hope that these results will stimulate theoretical work in this area. Moreover, our results suggest that the spectral density measured in the one-dimensional XY-like ferromagnetic CsNiF_3 in a parallel field should be interpreted in terms of breathers and magnons in contrast to current interpretation.¹⁰

^(a)Permanent address: Physics Department, Queen Mary College, Mile End Road, London, England.

¹T. Schneider and E. Stoll, Phys. Rev. Lett. **41**, 1429 (1978).

²M. J. Ablowitz, D. J. Kaup, A. C. Newell, and H. Segur, Phys. Rev. Lett. **30**, 1262 (1973).

³L. A. Takhtadzhyan and L. D. Faddeev, Theor. Mat. Fiz. **21**, 160 (1974).

⁴P. J. Caudrey, J. C. Eilbeck, and J. D. Gibbon, Nuovo Cimento B **25**, 447 (1975).

⁵R. F. Dashen, B. Hasslacher, and A. Neveu, Phys. Rev. D **11**, 3424 (1975).

⁶D. J. Kaup and A. C. Newell, Proc. Roy. Soc. London, Ser. A **361**, 413-446 (1978).

⁷T. Schneider and E. Stoll, Phys. Rev. B **17**, 1302 (1978).

⁸T. Schneider and E. Stoll, Phys. Rev. Lett. **31**, 1254 (1973).

⁹H. J. Mikeska, J. Phys. C **11**, L 29 (1978).

¹⁰M. Steiner and J. K. Kjems, in *Solitons and Condensed Matter Physics*, edited by A. R. Bishop and T. Schneider (Springer, Berlin and New York, 1978); J. K. Kjems and M. Steiner, Phys. Rev. Lett. **41**, 1137 (1978).

¹¹S. E. Trullinger, M. D. Miller, R. A. Guyer, A. R. Bishop, F. Palmer, and J. A. Krumhansl, Phys. Rev. Lett. **40**, 206, 1603(E) (1978).

¹²L. D. Landau and E. M. Lifschitz, *Physique Statistique* (Edition MIR, Moscow, 1967), p. 138.

Quark Structure Functions of Mesons and the Drell-Yan Process

Edmond L. Berger^(a) and Stanley J. Brodsky

Stanford Linear Accelerator Center, Stanford University, Stanford, California 94305

(Received 18 January 1979)

For massive-lepton pair production in meson-induced reactions, we use quantum chromodynamics perturbation theory to predict that the decay angular distribution in the pair rest frame will change from predominantly $1 + \cos^2\theta$ to $\sin^2\theta$ as the longitudinal-momentum fraction of the pair $x_F \rightarrow 1$. The two angular distributions are associated respectively with $(1-x)^2$ and $Q^{-2}(1-x)^0$ components of the valence-quark structure function of the meson.

The Drell-Yan process¹ $A + B \rightarrow l\bar{l}X$ measures the ability of colliding hadrons to reconfigure their momentum into the local production of a massive lepton pair with four-momentum Q^μ . As the edge of phase space is approached (i.e., $\tau = Q^2/s - 1$ or $x_F = Q_L/Q_L^{\max} - 1$), an annihilating quark q or antiquark \bar{q} in the subprocess $\bar{q}q \rightarrow \gamma^* \rightarrow l\bar{l}$ is taken far off-shell, and consequently the far-off-shell, short-distance internal dynamics of the hadronic wave function is probed. The Drell-Yan process can thus be used to determine the structure functions of hadrons not normally accessible in deep-inelastic scattering and to measure other important aspects of the dynamics

(e.g., spin properties) of the hadronic constituents at short distance.

In this Letter, we report an analysis of meson-induced massive-lepton pair production, $MB \rightarrow l\bar{l}X$, in the context of perturbative quantum chromodynamics (QCD). We go beyond the usual treatments by including explicit effects associated with the meson bound state.² We assume that in the low-momentum-transfer domain, the meson wave function describes a $q\bar{q}$ bound state, and that at large momentum transfer, the momentum dependence of the meson wave function is controlled by the Bethe-Salpeter kernel—and thus by single-gluon exchange in the asymptotic-

freedom limit. This idea is sketched in Fig. 1. The same model³ yields the standard predictions^{3,4} for the power behavior of meson and baryon form factors at large Q^2 , and for baryon valence structure functions, all consistent with experiment. Our focus here is on the consequences of the QCD description of internal hadron dynamics; logarithmic corrections due to QCD radiative processes can be treated in the conventional manner.

The most striking testable consequences of this QCD picture for $MB \rightarrow l^+l^-X$ are its predictions for the valence-quark structure function of the meson and for the polarization of the virtual photon $\gamma^* \rightarrow l^+l^-$. The structure function has both a scaling⁵ $[(1-x)^2]$ and a nonscaling⁶ $[Q^{-2}(1-x)^0]$ component, with specified relative magnitude. Each is associated with a different angular distribution in the lepton-pair rest frame. For $Mq \rightarrow l^+l^-X$, we obtain

$$d\sigma \propto (1-x)^2(1 + \cos^2\theta) + \frac{4}{9}(\langle k_T^2 \rangle / Q^2) \sin^2\theta. \quad (1)$$

Here x is the momentum fraction (light-cone variable) of the annihilating \bar{q} from the meson, $\langle k_T^2 \rangle$ is the average of the square of its transverse momentum, and $\cos\theta = \hat{p}_l \cdot \hat{p}_\pi$ is defined in the lepton-pair rest frame. Identification of the nonscaling piece in the data can be made in several different ways: the x dependence of the cross section at fixed Q^2, s ; the angular (θ) dependence at fixed x, Q^2, s ; and the s dependence at fixed Q^2/s .

The dominant contribution to $\pi^- N \rightarrow \mu^+ \mu^- X$ at large Q^2 arises from the annihilation $\bar{u}u \rightarrow \gamma^* \rightarrow \mu^+ \mu^-$, where the antiquark \bar{u} comes from the π^- and the u from the nucleon. We concentrate on the kinematic region where only the \bar{u} is far off-shell (i.e., $x_F \rightarrow 1$). It is sufficient to treat the u quark as nearly free and on-shell. Thus, the incident nucleon structure is not indicated in the lowest-order diagrams shown in Fig. 1 for $\pi^- q \rightarrow \gamma^* q$. Both diagrams in Fig. 1 are required by gauge invariance, although in a physical (axial) gauge, the scaling contributions as $Q^2 \rightarrow \infty$ can be identified solely with Fig. 1(a). We partition the

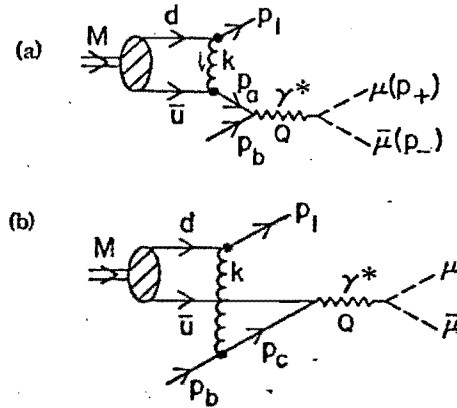


FIG. 1. Diagrams for $Mq \rightarrow q\gamma^*$, $\gamma^* \rightarrow \mu^+\mu^-$. Solid single lines represent quarks. Symbols p_1, p_a, p_b , and p_c denote four-momenta of quarks, and k is the four-momentum of the gluon.

incident meson momentum p equally between the constituent q and \bar{q} ; this simplifying approximation can be discarded as it does not affect our conclusions.

The kinematics of the annihilating antiquark are specified with light-cone variables $x_a = (p_a^0 + p_a^3) / (p^0 + p^3)$, and k_{Ta} . Setting $p_a^2 = m^2$, where m denotes the bare quark mass, we use energy and momentum conservation to derive

$$p_a^2 = - \frac{\bar{k}_{Ta}^2 + x_a m^2 - x_a(1-x_a)m_\pi^2}{1-x_a}. \quad (2)$$

As $x_a \rightarrow 1$, p_a^2 becomes large and far spacelike. The squared four-momentum carried by the gluon in Fig. 1,

$$k^2 = (p_1 - \frac{1}{2}p)^2 = \frac{1}{2}(p_a^2 + m^2) - \frac{1}{4}m_\pi^2,$$

also becomes large as $x_a \rightarrow 1$. Therefore, invoking arguments based on asymptotic freedom, we suppose that in the range of x_a of interest to us, the single-gluon-exchange approximation shown in Fig. 1 will yield a good representation of the asymptotic large-momentum behavior of the Bethe-Salpeter kernel for the $q\bar{q}$ bound state.⁷

The invariant amplitude corresponding to Fig. 1 is

$$\mathfrak{M} \propto \bar{u}(p_+) \gamma_\mu v(p_-) \frac{1}{Q^2} \frac{\alpha_s \langle k^2 \rangle}{k^2} \psi_\pi(0) \sum_\lambda \bar{u}(p_+) \gamma_\alpha u_\lambda(\frac{1}{2}p) \bar{v}_\lambda(\frac{1}{2}p) \left[-\gamma^\alpha \frac{1}{\not{p}_a + m} \gamma^\mu + \gamma^\mu \frac{1}{\not{p}_c - m} \gamma^\alpha \right] u(p_b), \quad (3)$$

where $\sum_\lambda u_\lambda \bar{v}_\lambda = (\frac{1}{2}\not{p} + m)\gamma_5$ specifies that the $\bar{u}q$ bound state is a pseudoscalar.⁸ The factor $\psi_\pi(\vec{x}=0)$ in Eq. (3) represents an integration over the soft momenta in the pion wave function. We remark that our expression for the amplitude is precisely correct in the limit of zero binding energy for the meson. Note also that in our calculation the quark transverse momentum \bar{k}_T enters explicitly; it is not an arbitrarily assigned "intrinsic" or "primordial" \bar{k}_T associated with the $q\bar{q}$ binding in the wave function.

For simplicity in what follows, we set $m^2=0$ and $m_\pi^2=0$, and we restrict our attention to $\bar{k}_{T_a}^2 \ll Q^2$. Using the amplitude in Eq. (3), we compute an explicit expression for the cross section for $\pi^- N \rightarrow \mu^+ \mu^- X$. After integration over the azimuthal angle in the pair rest frame, we obtain

$$\frac{Q^2 d\sigma}{dQ^2 d^2k_T dx_L d\cos\theta} \propto \int d^2k_{T_a} dx_a d^2k_{T_b} dx_b G_{q/N}(x_b, \bar{k}_{T_b}) \frac{\psi_\pi^2(0)}{k_{T_a}^4} \left[(1-x_a)^2 (1+\cos^2\theta) + \frac{4k_{T_a}^2}{9Q^2} \sin^2\theta \right] \times \delta^{(2)}(\bar{Q}_T - \bar{k}_{T_a} - \bar{k}_{T_b}) \delta(x_L - x_a - x_b) \delta(Q^2 - x_a x_b s). \quad (4)$$

Here $G_{q/N}$ is the quark structure function of the nucleon. We have discarded contributions which are of order $Q^{-2} k_T^2 (1-x_a)$ and $Q^{-4} k_T^4 (1-x_a)^{-1}$ in the square brackets of Eq. (4).⁹ The contributions from sea quarks and antiquarks in the meson and nucleon are also ignored in Eq. (4).

In the Bjorken scaling limit, $Q^2 \rightarrow \infty$, at fixed x_a , the valence-quark structure function can be extracted from Eq. (4):

$$G_{\bar{q}/\pi}(x) = \int d^2k_T G_{\bar{q}/\pi}(x, \bar{k}_T) \propto (1-x)^2. \quad (5)$$

The corresponding \bar{k}_T falloff produces pairs with a Q_T^{-4} distribution² (for $k_{T_a}^2 \ll Q^2$).

We observe the following additional features of Eq. (4): (i) We can identify a nonscaling contribution to the structure function. After averaging over $\cos\theta$, we obtain

$$G_{\bar{q}/\pi} \rightarrow (1-x)^2 + \frac{2}{9} \langle k_{T_a}^2 \rangle / Q^2. \quad (6)$$

The nonscaling contribution is independent of x and will dominate the scaling contribution at fixed $Q^2(1-x)$ as $Q^2 \rightarrow \infty$. In our model the relative magnitude of the scaling and nonscaling terms is fixed.⁹ When the nonscaling term dominates in Eq. (4), the mean $\langle k_{T_a}^2 \rangle$ is of order $Q^2/\ln Q^2$.

(ii) The nonscaling contribution corresponds to a longitudinal structure function and provides a $\sin^2\theta$ angular distribution in the lepton-pair rest frame, in contrast to the conventional expectation of $1+\cos^2\theta$. At fixed Q^2 , the $\sin^2\theta$ term dominates in the cross section as $x_F \rightarrow 1$. The usual rule that annihilating spin- $\frac{1}{2}$ quarks produce transversely polarized photons is modified when off-shell constituents are involved. In our case, the \bar{q} is kinematically far off shell since, as $x_F \rightarrow 1$, all of the momentum of the recoil spectator quark must be transferred to the annihilation subprocess. In this situation the spin of the incident meson influences the final angular distribution. In a different language, the bound-state effect can be identified with a "high-twist" subprocess, since more than the minimum number of elementary fields is required.

In the range $4.0 \leq M = (Q^2)^{1/2} \leq 8.5$ GeV, an effective pion structure function has been extracted by Newman *et al.*¹⁰ from their data on $\pi^- N \rightarrow \mu^+ \mu^- X$

at 225 GeV/c. They report that $x G_{\pi}^{\text{exp}}(x) \approx 0.5(1-x)^{1.01 \pm 0.05}$ for $x > 0.3$. For similar values of Q^2 , our structure function in Eq. (6) can mimic the observed $(1-x)^1$ behavior if we choose $\langle k_{T_a}^2 \rangle \approx 1$ GeV². This value of $\langle k_{T_a}^2 \rangle$ is consistent with measured¹⁰ values of $\langle Q_T^2 \rangle = \langle (\bar{k}_{T_a} + \bar{k}_{T_b})^2 \rangle$. We remark parenthetically that the parameter $\langle k_{T_a}^2 \rangle$ in our formulas is a function of Q^2 and x and effectively includes the mass terms which were dropped when we set m^2 and $m_\pi^2 = 0$. Shown in Fig. 2(a) is a comparison of our structure function, Eq. (6), for different values of Q^2 , with the form $G_{\pi}^{\text{exp}}(x)$ deduced from the data, assuming Q^3 independence. We urge that the analysis of the data be repeated with Eq. (6).

In Fig. 2(b) we present our prediction for the polarization parameter α in the expression $d\sigma/d\cos\theta = 1 + \alpha \cos^2\theta$. In our model, $\alpha = (1-r)/(1+r)$, with

$$r = \frac{4}{9} \langle k_{T_a}^2 \rangle / Q^2 (1-x_a)^2. \quad (7)$$

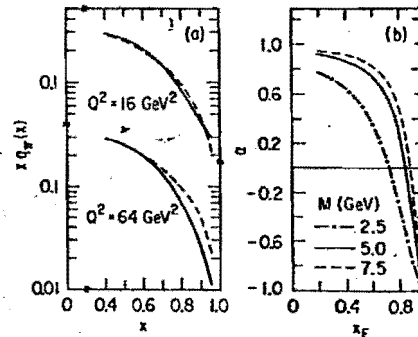


FIG. 2. (a) The quantity $xq_\pi(x)$ as a function of x for two values of Q^2 near the top and bottom of the range explored experimentally. Here we set $xq_\pi(x) = 2xG_{\bar{q}/\pi}$ with $G_{\bar{q}/\pi}$ provided in Eq. (6), and $\langle k_{T_a}^2 \rangle = 1$ GeV². The factor 2 is chosen to reproduce approximately the normalization of the experimentally deduced effective $xq_\pi(x)$ near $x=0.5$. For comparison, we plot as a dashed curve the experimental form (Ref. 10) $0.5(1-x)^{1.01}$. The computations in this paper are applicable only for $x > 0.5$. (b) Predicted value of α as a function of x_F for different values of $M = (Q^2)^{1/2}$ at $p_{\text{lab}} = 225$ GeV/c, with $\langle k_{T_a}^2 \rangle = 1$ GeV².

Our predictions are presented as a function $x_F = (x_a - \tau/x_a)/(1 - \tau)$. The angle θ is referred to the t -channel (or Gottfried-Jackson) system of axes: $\cos\theta = \hat{p}_\mu \cdot \hat{p}_\pi$. Observed values of α are reported¹⁰ only for data averaged over all x_F , and, as we expect in this case, $\alpha \approx 1$ for $4 < M < 8.5$ GeV.

The experimental observation of an effective $(1-x)^1$ behavior of the quark structure function of the pion is incompatible with general crossing arguments for Born diagrams which mandate only even powers of $1-x$ as $x \rightarrow 1$ when a fermion is extracted from a meson.¹¹ The linear behavior $(1-x)$ would be expected, of spinless quarks. On the other hand, the spin- $\frac{1}{2}$ nature of the constituents seems well established by the observation in the same experiment of a decay angular distribution of $1 + \alpha \cos^2\theta$ with $\alpha \approx 1$. Our analysis provides a resolution of this apparent paradox. We suggest that the observed $(1-x)^1$ behavior is an approximation to our Eq. (6), in which only even powers of $1-x$ appear. The critical test of this assertion is the identification of the predicted $\sin^2\theta$ behavior of the decay angular distribution at large x_F .

Observation of our predicted $\sin^2\theta$ nonscaling term in the data would reinforce the applicability of the Drell-Yan model with spin- $\frac{1}{2}$ quarks and verify that structure functions can be understood in some detail in a QCD framework. Failure would mean that there is no fundamental explanation for the observed power behavior of structure functions. The nonscaling and angular-dependent effects we derive are in addition to, but much stronger than, analogous effects provided by QCD gluonic radiative corrections; in particular, our prediction for the angular distribution applies at small Q_T , where gluonic radiative corrections do not upset the conventional $1 + \cos^2\theta$ expectation.¹² The form we derive for the structure function in Eq. (6) should apply universally; for example, an analogous structure function should also be observed in meson-induced large- p_T hadronic processes.¹³

In baryon- (or antibaryon-) induced reactions, $BB \rightarrow \bar{U}X$, the $1 + \cos^2\theta$ behavior characteristic of spin- $\frac{1}{2}$ systems is maintained as $x \rightarrow 1$. However, nonscaling longitudinal contributions arise near $x = \frac{2}{3}$ if we take into account the subprocess $(qq) + \bar{q} \rightarrow q + \gamma^*$ with a bosonic diquark system.¹⁴ These effects may be related to the anomalous values of σ_L/σ_T observed in deep-inelastic electron scattering¹⁵ at moderate values of Q^2 .

We thank R. Blankenbecler for helpful conver-

sations.

^(a) Permanent address: High Energy Physics Division, Argonne National Laboratory, Argonne, Ill. 60439.

¹S. D. Drell and T.-M. Yan, *Phys. Rev. Lett.* **25**, 316, 902(E) (1970). For a recent review see E. L. Berger, in *New Results in High Energy Physics*, AIP Conference Proceedings No. 45, edited by R. S. Panvini and S. E. Csorna (American Institute of Physics, New York, 1978).

²M. Duong-van, K. V. Vasavada, and R. Blankenbecler, *Phys. Rev. D* **16**, 1389 (1977); C. Debeau and D. Silverman, SLAC Report No. SLAC-PUB-2187, 1978 (unpublished).

³S. J. Brodsky and G. R. Farrar, *Phys. Rev. Lett.* **31**, 1153 (1973), and *Phys. Rev. D* **11**, 1309 (1975).

⁴V. A. Matveev, R. M. Muradyan, and A. N. Tavkhelidze, *Lett. Nuovo Cimento* **7**, 719 (1973).

⁵Z. F. Ezawa, *Nuovo Cimento* **23A**, 271 (1974).

⁶G. R. Farrar and D. R. Jackson, *Phys. Rev. Lett.* **35**, 1416 (1975). Our results are analogous to those for $e^+e^- \rightarrow \pi X$ derived by Farrar and Jackson. However, in the Drell-Yan process, the dominance of the longitudinal term at large x cannot be attributed to exclusive channels. See also A. I. Vainshtain and V. I. Zakharov, *Phys. Lett.* **72B**, 368 (1978).

⁷See, e.g., T. Appelquist and E. Poggio, *Phys. Rev. D* **10**, 3280 (1974), and Ref. 3. A detailed discussion will be given by S. J. Brodsky and P. Lepage, to be published. For a similar problem in quantum electrodynamics, see W. Caswell and P. Lepage, *Phys. Rev. A* **18**, 810 (1978).

⁸Our results also hold when the quark spins are uncorrelated.

⁹Our results are accurate in two $Q^2 \rightarrow \infty$ limits: (a) the fixed- x_B Bjorken limit, and (b) the fixed- $W^2 = (1-x)Q^2/x$ limit, with $W^2 \gg k_T^2$. The neglected terms in Eq. (4) must be retained at modest Q^2 for x very close to 1 ($\rho > 0.95$).

¹⁰C. B. Newman *et al.*, *Phys. Rev. Lett.* **42**, 951 (1979) (this issue), and private communications.

¹¹S. D. Drell, D. J. Levy, and T.-M. Yan, *Phys. Rev. D* **1**, 1617 (1970). For a discussion of non-Born diagrams, see P. V. Landshoff and J. C. Polkinghorne, *Phys. Rev. D* **6**, 3708 (1972).

¹²K. Kajantie, J. Linfors, and R. Raitio, *Phys. Lett.* **74B**, 384 (1978); E. L. Berger, J. T. Donohue, and S. Wolfram, *Phys. Rev. D* **17**, 858 (1978); Berger, Ref. 1.

¹³A measurement of the quark structure function of the pion as seen in pion-induced hadronic jets is reported by M. Dris *et al.*, Pennsylvania University Reports No. UPR-39E (Rev.) and No. UPR-55E, 1978 (unpublished).

¹⁴In deep-inelastic processes, $\gamma^* + (qq)$ subprocesses have been considered by I. A. Schmidt, Ph.D. thesis, Stanford University SLAC Report No. 203, 1977 (unpublished); I. A. Schmidt and R. Blankenbecler, *Phys. Rev. D* **16**, 1318 (1977).

Supplement to Proposal 615

A Study of the Forward Production of Massive Particles

C. Adolphsen, K. J. Anderson, K. P. Karhi, J. E. Pilcher, E. I. Rosenberg
Enrico Fermi Institute, University of Chicago
Chicago, Illinois 60637

and

J. Elias

Fermi National Accelerator Laboratory, Batavia, Illinois 60510

and

K. T. McDonald, A.J.S. Smith

Joseph Henry Laboratories, Princeton University, Princeton, NJ 08540

Supplement to P-615

I. INTRODUCTION

This supplement is intended to provide details about the experiment beyond those given in the original proposal. Among the items discussed in more detail are acceptances, resolution, counting rates, specific physics goals and how the experiment might be implemented.

II. APPARATUS

The schematic of the detector is reproduced from the original proposal in Fig. 1. For performance calculations we have taken the mass selection magnet to be 8.5 m long, 0.76 m (30 in.) wide, and with a final gap height of 0.76 m. The field is taken as uniform with a maximum value of 15.7 kG. As mentioned in the proposal, this system could be based on 4 ANL beam line dipoles with the gaps opened and additional excitation. The cost of this and other alternatives are being estimated by the Meson Department and should be available by the March PAC meeting. For purpose of comparison we note that this magnet system has less than one-half the field volume of the M2 magnet requested in P-605.

The analyzing magnet shown in Fig. 1 is similar to the magnet designed for E-516 (Nash). It has a P_T kick of 0.5 GeV/c and an aperture of 2 m x 1 m. The field volume of this magnet is less than one-tenth the volume of the P-605 analyzing magnet.

(a) Acceptance

The acceptance of the system has been studied as a function of several parameters.

The acceptance is most directly controlled by changing the aperture of the downstream slit and the field in the mass selecting dipole. Figure 2 shows the absolute acceptance as a function of slit width at a mass of 1.86 and 4.0 GeV for a series of field settings. The field is characterized by a constant, S , which is the P_T kick of the mass selector compared to twice the maximum P_T available from the particle decay. Thus for $S=1$, decays which are exactly transverse to the beam and in the bend plane are brought to a focus at the slit. The acceptance calculation assumes a t -distribution for the forward going particle of $dN/dt \sim e^{-3.5|t'|}$ as suggested by Field and Quigg for associated charmed meson, charmed baryon production.

It is seen from Fig. 2 that the acceptance grows linearly with slit width. As discussed below, the single arm fluxes rise faster than linear as the slit width is opened and these rates impose the upper limit on the opening.

It is also relevant to consider the shape of the mass acceptance for various slit openings and a fixed magnetic field. This is given in Fig. 3. In considering these shapes it should be recalled that the mass resolution is $\sim 8 \text{ MeV}/c^2$.

For the calculations discussed below we adopt a slit width of 20 cm. and a field setting of $S=0.90$.

Massive forward going particles may be produced with a fairly broad t -distribution. Figure 4 shows the acceptance as a function of $|t'| = |t - t_{\min}|$. For comparison, a t -distribution of $e^{-3.5|t'|}$ is plotted. The acceptance in t is good, falling a factor of four over the same interval in which the trial distribution falls a factor of 10.

Figure 5 shows the acceptance at different mass settings for fixed slit width and S -value. It should be possible to open the slit at the higher mass settings since the single particle backgrounds are smaller at these P_T values.

(b) Mass Resolution

For the resolution calculation we assume that the PWC system indicated in Fig. 1 provides 2 X and 2 Y measurements at each of the two detector stations upstream of the analyzing magnet. At the two downstream stations 1 X and 1 Y measurement is used. The wire spacing is taken to be 1.6 mm, similar to other PWC's built at the Enrico Fermi Institute. A target of 0.2 absorption lengths of beryllium (7.4 cm.) is used.

With this system we obtain a resolution which is limited by the incident beam size and multiple scattering in the target. With a beam size of $\sigma_x = 0.75$ mm. (see Cary report) and no multiple scattering, the resolution is $\sigma_m = 2$ MeV at $M = 1.86$ GeV (0.1%). With the same beam size and multiple scattering $\sigma_m = 8$ MeV (0.4%). With a beam of $\sigma_x = 1$ cm. and multiple scattering the mass resolution is $\sigma_m = 16$ MeV (0.9%). No contribution is included for uncertainty in the field integrals but fortunately the track trajectories in this experiment are contained in only a small fraction of the phase space volume which could be transported by the magnets.

The mass resolution is plotted as a function of mass in Fig. 6 with the small beam size and multiple scattering included.

III. COUNTING RATES

An item not discussed in the original proposal is the single arm counting rate to be expected at 2×10^9 interacting pions/pulse. Figure 7 shows the expected single arm rate as a function of slit width if the mass acceptance is centered at 1.86 GeV. To calculate these rates, measured single particle inclusive cross sections are parametrized in the appropriate region of x_F and P_T and used as input to a Monte Carlo simulation of the mass selector. A single arm flux of $4 \times 10^6 / 2 \times 10^9$ interacting pions is obtained with a slit width of 20 cm.

It should be noted that a simple arm-to-arm coincidence is not used since most random two particle combinations lie outside the kinematic regions of interest (x_F , M , P_T of the pair). Instead, fast matrix logic together with hardware processors will be used to select pairs of interest. This technique has already been exploited by this group in its μ -pair studies (E-444).

If the field in the mass selecting dipole is raised to center the acceptance at a 4 GeV mass, the single arm fluxes fall by over two orders of magnitude.

IV. IMPLEMENTATION

The cost estimates given in this section are current best estimates developed in consultation with the Meson Department. More accurate figures may appear by the time of the PAC meeting.

(a) Mass Selection Dipole

As described above one way to construct this magnet system is to base it on four ANL beam line dipoles with the gaps of three, opened and additional coils added. The cost of copper coils for this option has been estimated by the Meson Department at \$300K. The additional machined steel costs \$12K (\$250/ton) so that, with labor included, the new cost for this magnet system is put at \$325K. The question of power is discussed below but the conclusion is that with the beam operating at 50 GeV and focused to an upstream enclosure, there are sufficient power supplies and electrical energy from the present configuration of the M1 line.

Naturally we would be happy to consider other alternatives for constructing this magnet but they should be competitive with the cost and time scale of this solution.

(b) Analyzing Magnet

A magnet similar to the one required has been designed for E-516 (Nash) in the Tagged-Photon Lab. This magnet has an aperture of 72 in. x 32 in. (1.82 m x 0.81 m) and a P_T kick of 0.46 GeV/c. The area of the aperture is ~75% of that used for the efficiency calculations above, and the P_T kick is over 90% of that used. The proposed experiment could certainly be tailored to use a magnet of these dimensions.

The cost of this magnet is ~\$200K and the power requirement is 475 kw.

(c) Location

A solution which would permit the experiment to coexist with P-605 would be to build an upstream experimental enclosure, similar to that considered for P-586 (McCarthy). A beam can be constructed from existing M1 components which would produce high flux pions to this upstream enclosure and with minor modifications deliver 400 GeV protons to the Meson Detector Building for Phase I of P-605.

The idea is to concentrate most of the quadrupoles in the upstream section and relatively few in the downstream section where only primary protons are to be transported. Since the beam is to be operated at 50 GeV for P-615, the extra electrical power would be used for the mass selecting dipoles.

An example of a possible beam configuration is the first half of the beam described in the Cary report. The exact design must be tailored to the existing tunnels.

VI. PHYSICS GOALS

The primary goal of this experiment is to scan the two particle mass spectrum from 1.5 to 5 GeV. Special emphasis will be given to $K\pi$ masses close to 1.86 GeV (charmed meson production) and to $\bar{p}p$ masses in the range 2.8 to 3.1 GeV where the η_c may be expected.

Figure Captions

- Fig. 1. A schematic drawing of the apparatus.
- Fig. 2. Acceptance at mass settings of 1.86 and 4.0 GeV for various slit widths and field settings. The constant S is the P_T kick of the magnet compared to that required for perfect focussing of an exactly transverse decay in the bend plane.
- Fig. 3. Shape of the mass acceptance as a function of slit width for a given field setting. All curves have been normalized to the same peak amplitude. The relative normalizations can be obtained from Fig. 2.
- Fig. 4. Acceptance as a function of $|t'|$ of the forward going particle. For comparison a possible t' distribution for production is also shown. A slit width of 20 cm. and an S -value of 0.9 has been used for these calculations.
- Fig. 5. Acceptance for various mass settings at a fixed slit width of 20 cm. and a field setting of $S=0.9$.
- Fig. 6. Mass resolution as a function of mass. A beam size of $\sigma_x = 0.75$ mm and a 0.2 absorption length beryllium target are assumed.
- Fig. 7. Single arm counting rate as a function of slit width for 2×10^9 interacting pions per second of spill.

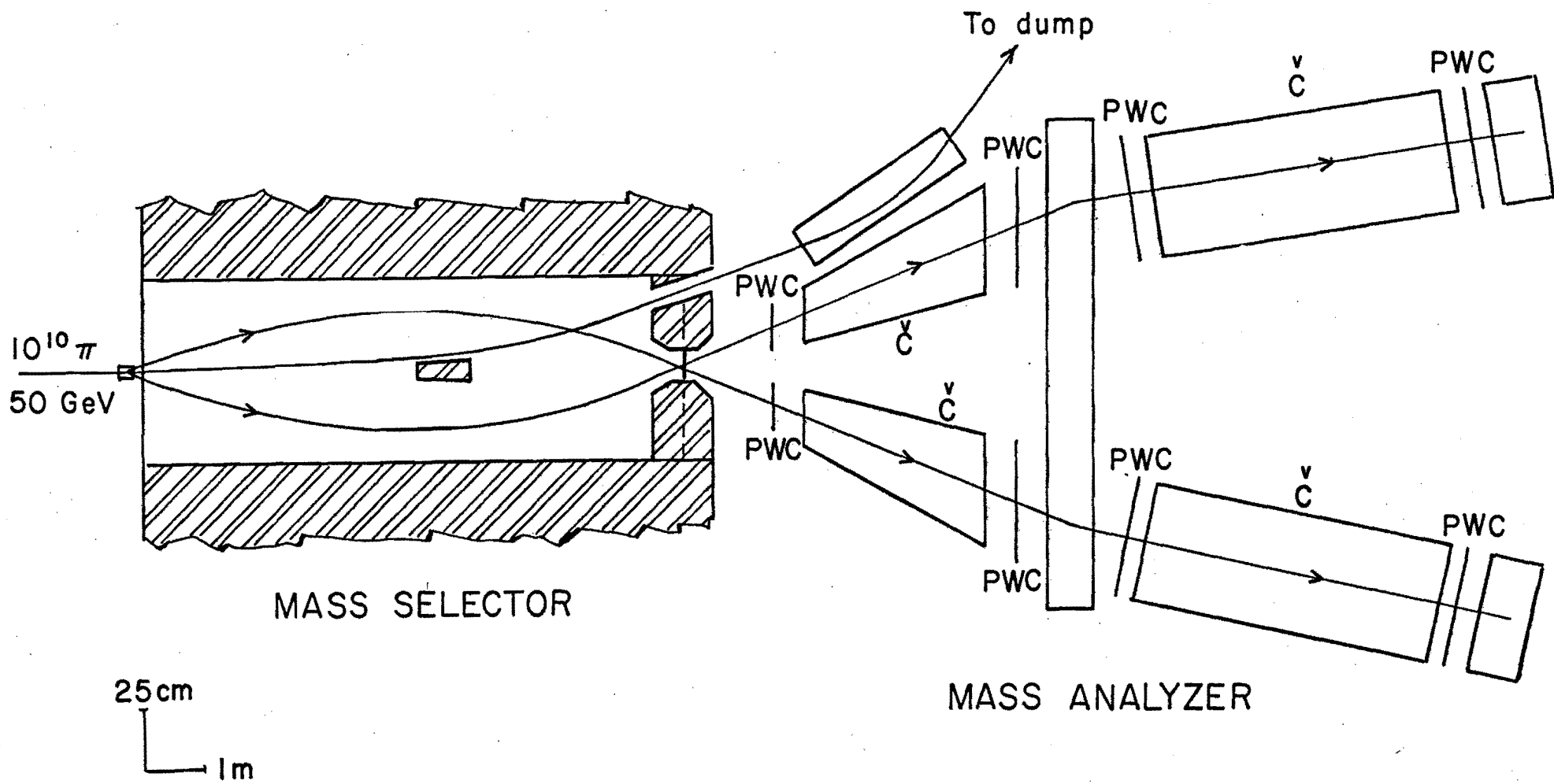


Figure 1

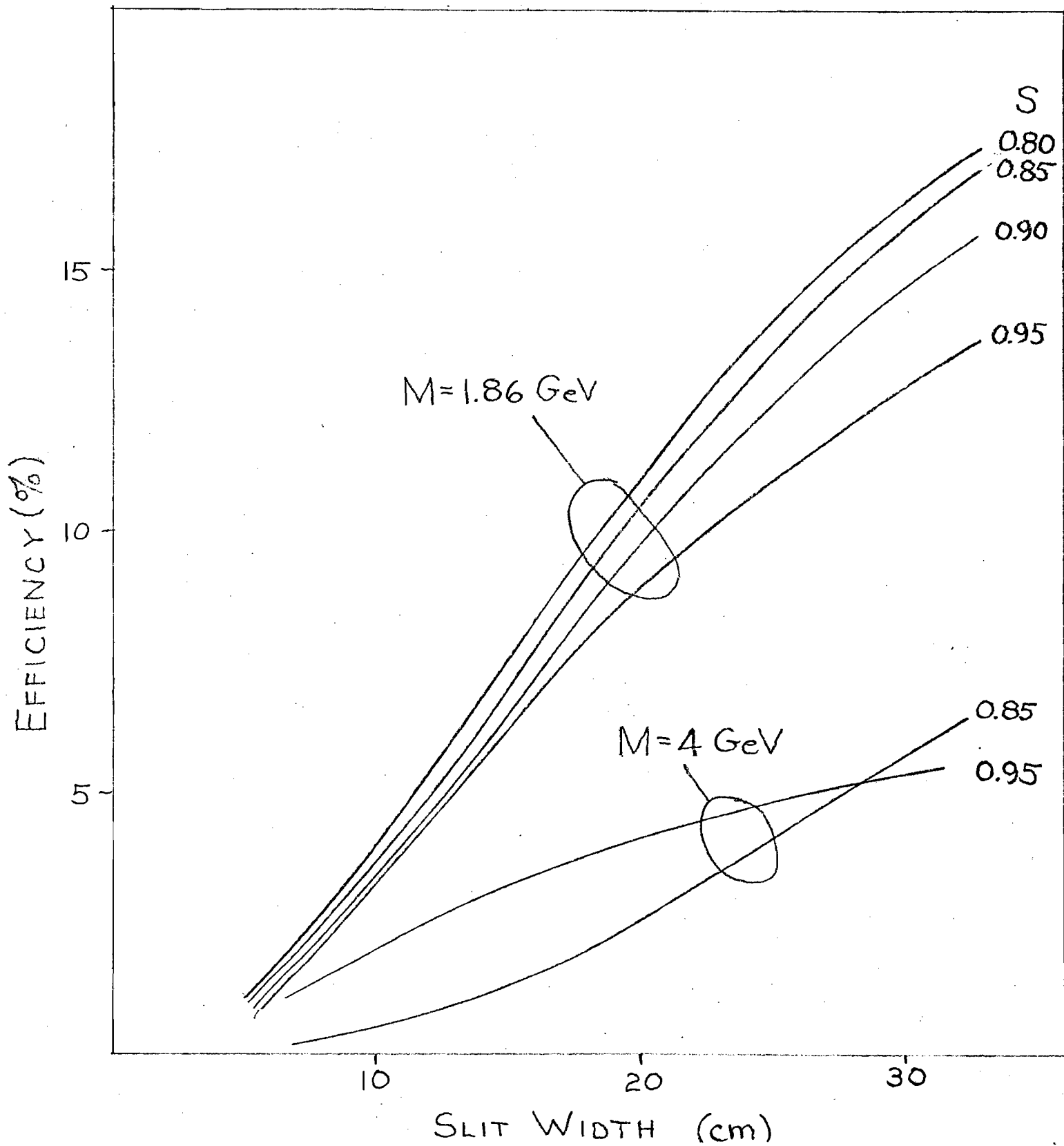


Figure 2

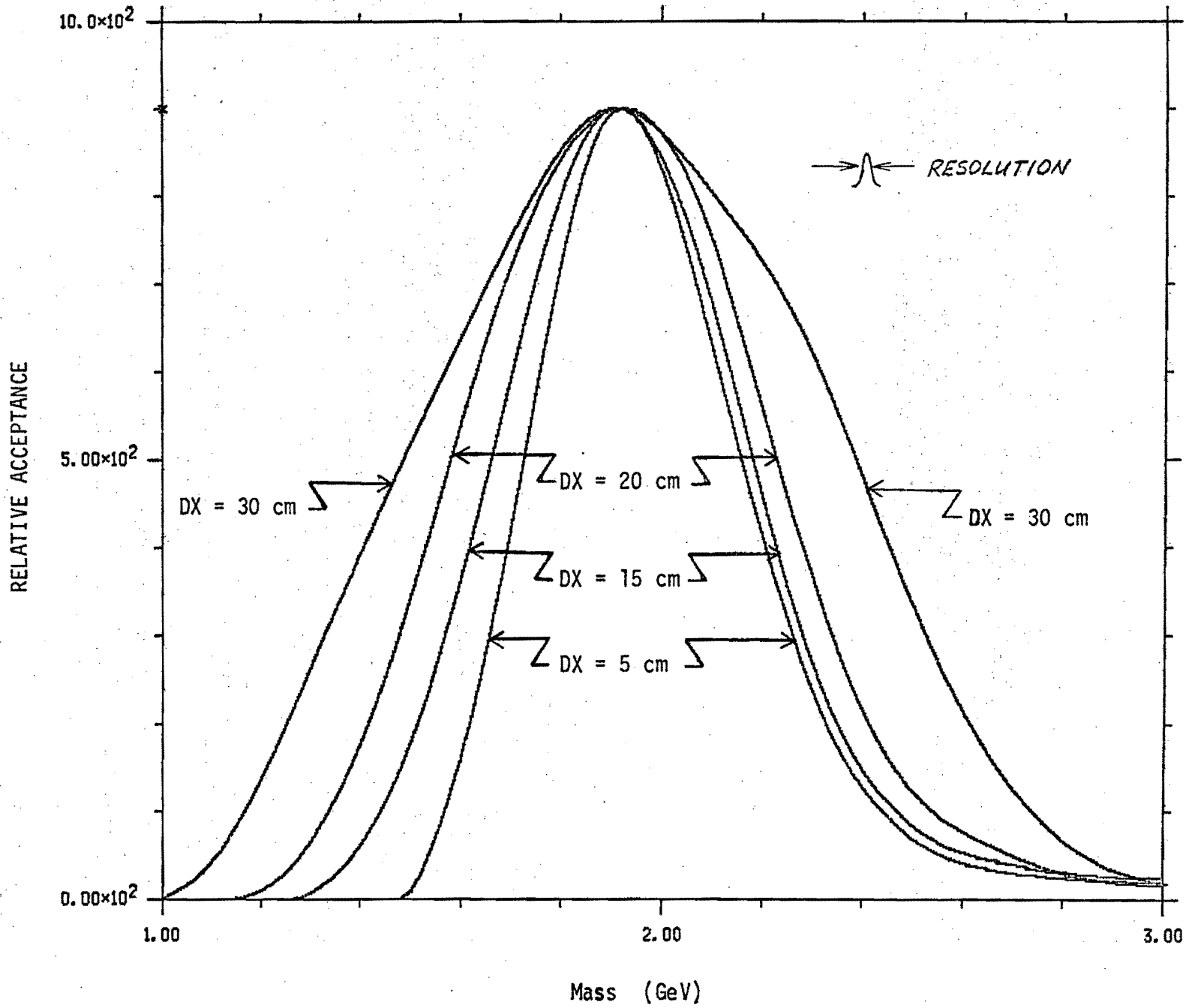


Fig. 3

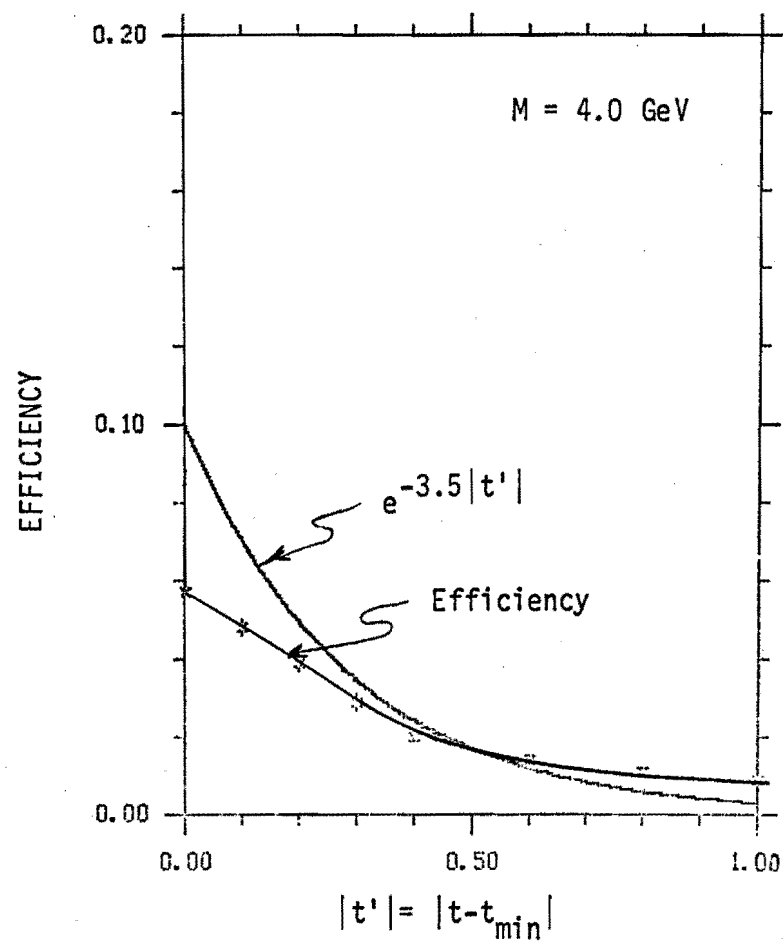
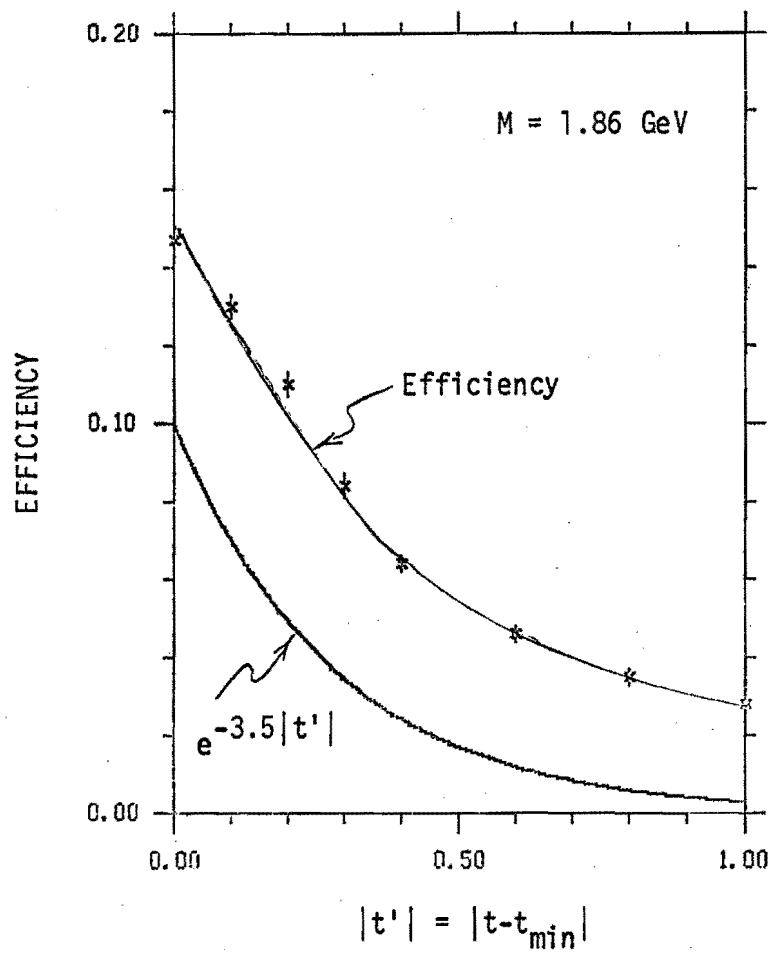


Fig. 4

ACCEPTANCE VS MASS

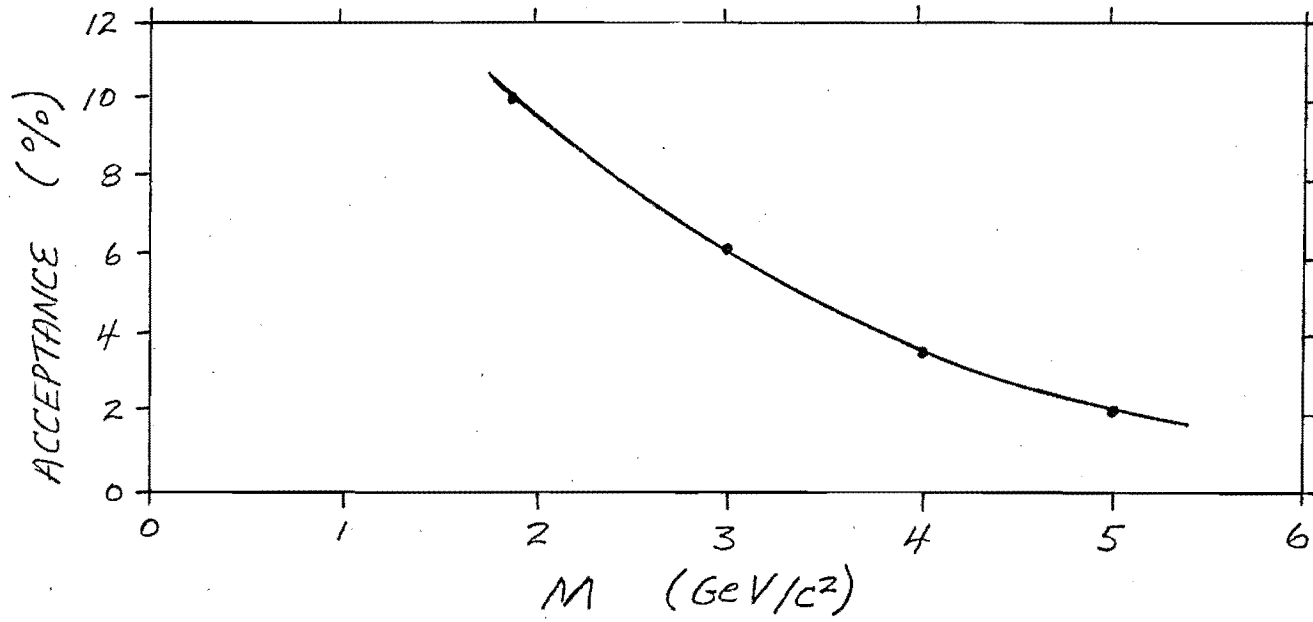


Fig. 5

RESOLUTION VS MASS

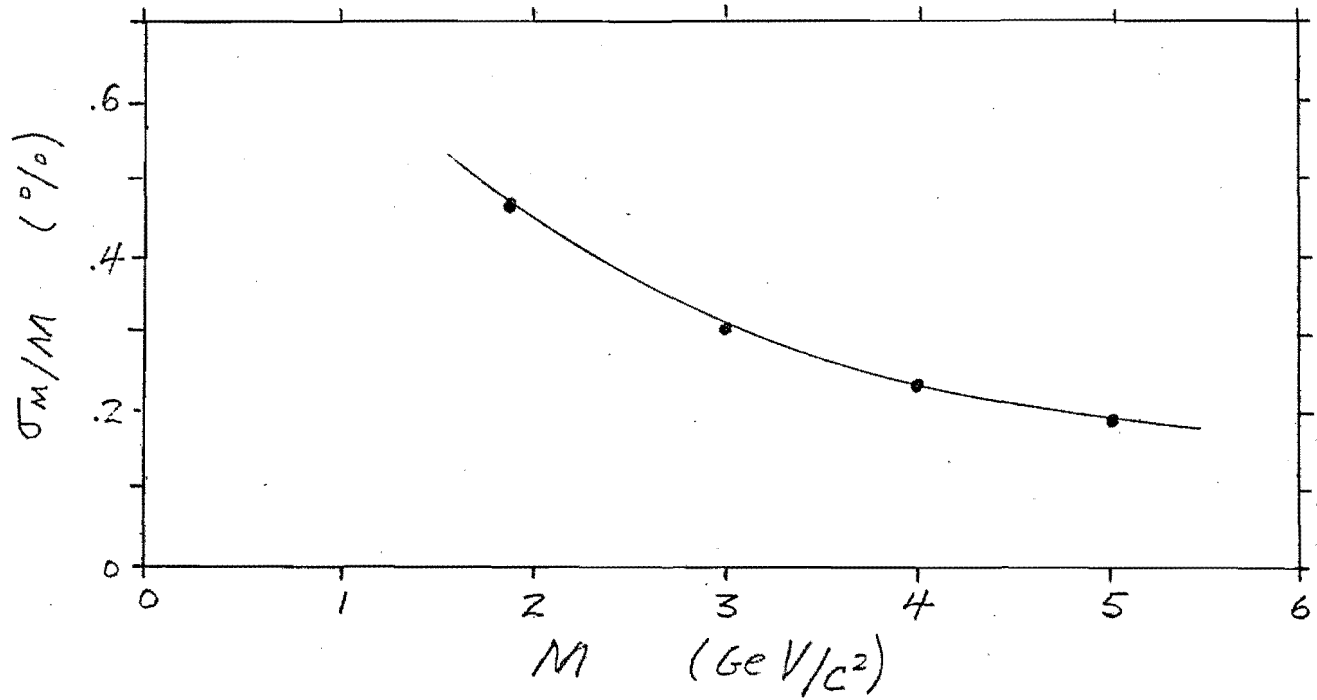


Fig. 6

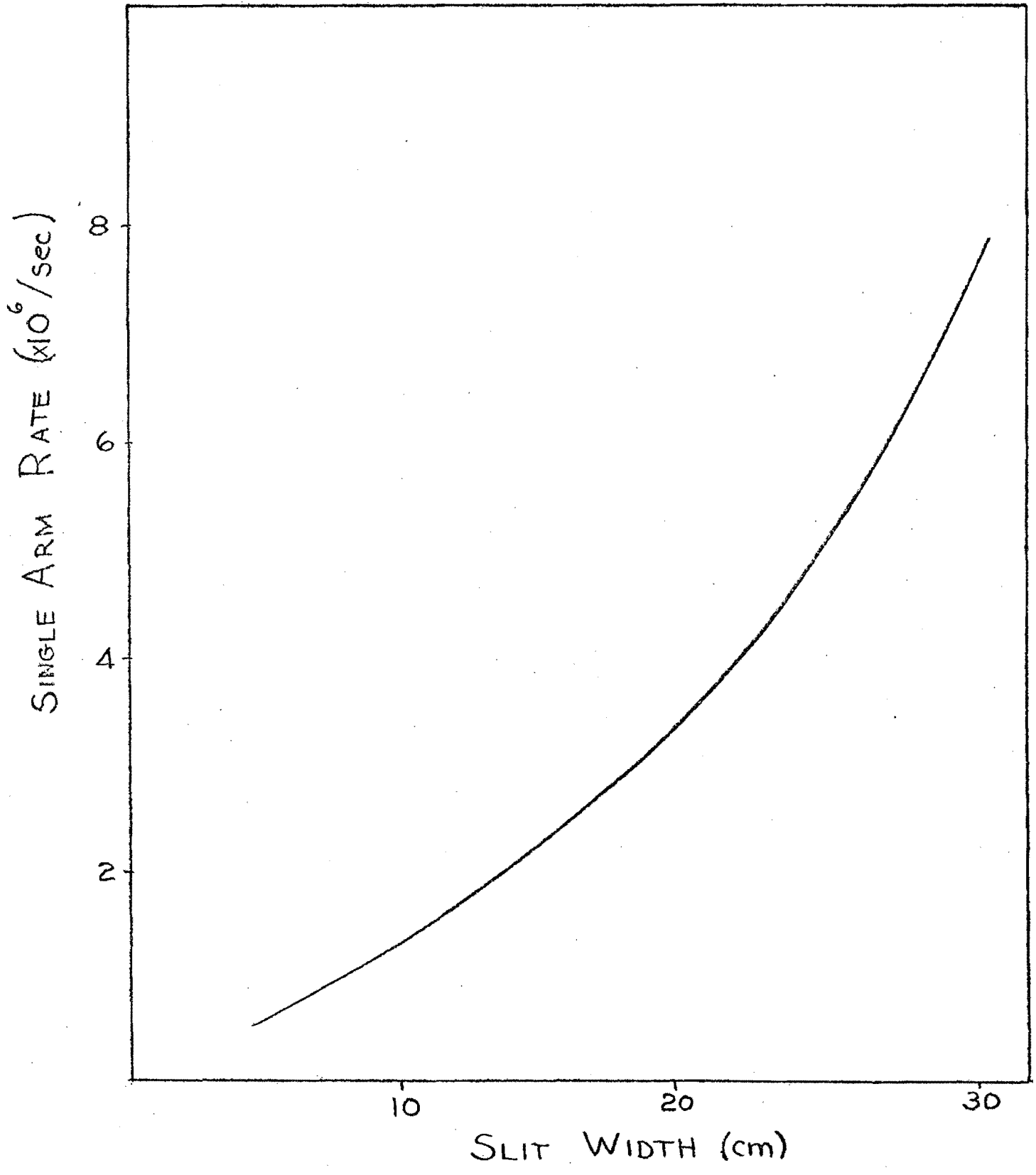


Figure 7